Chem Soc Rev

This article was published as part of the

2009 Metal–organic frameworks issue

Reviewing the latest developments across the interdisciplinary area of metal–organic frameworks from an academic and industrial perspective

Guest Editors Jeffrey Long and Omar Yaghi

Please take a look at the issue 5 table of contents to access the other reviews.

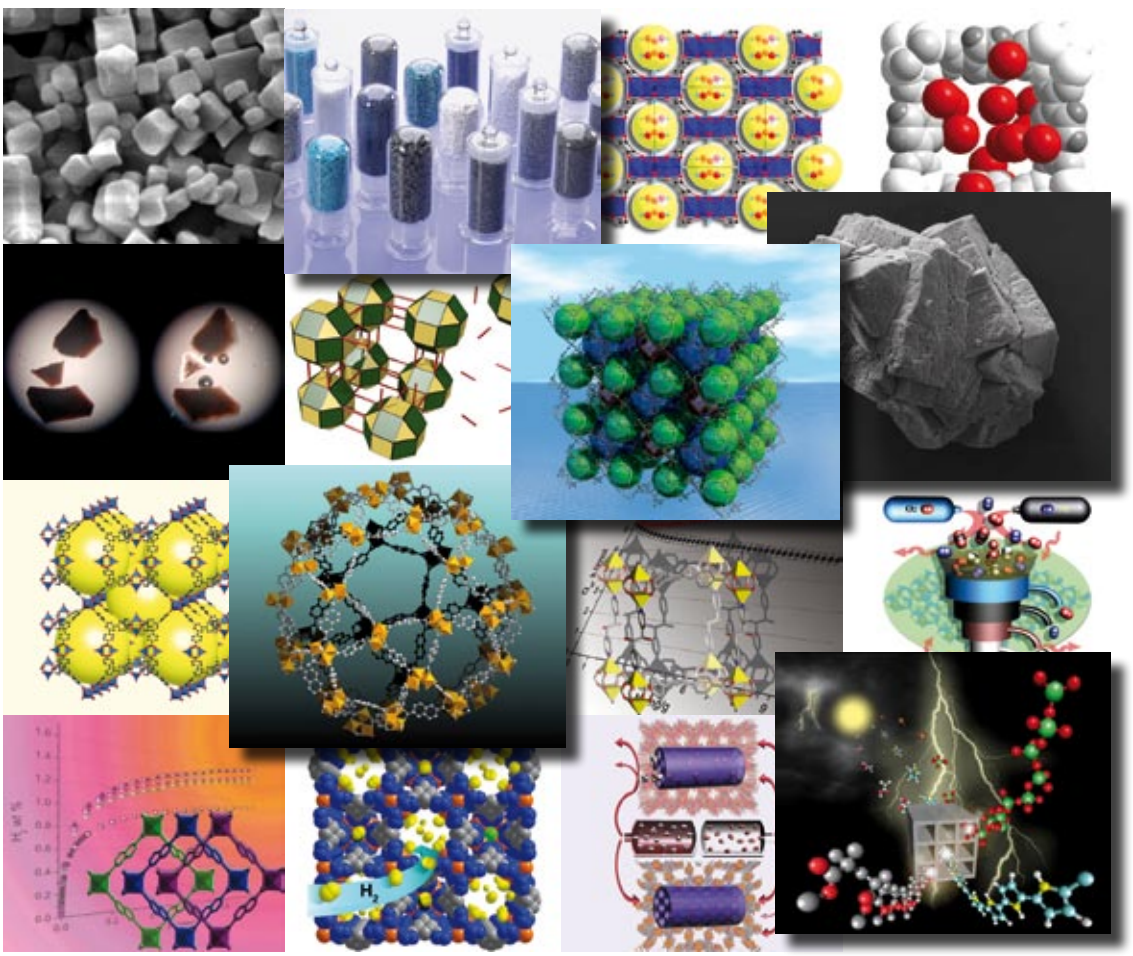

Recent advances on simulation and theory of hydrogen storage in metal–organic frameworks and covalent organic frameworks†

Sang Soo Han,‡ José L. Mendoza-Cortés and William A. Goddard III*

Received 28th January 2009
First published as an Advance Article on the web 24th March 2009
DOI: 10.1039/b802430h

This *critical review* covers the application of computer simulations, including quantum calculations (*ab initio* and DFT), grand canonical Monte-Carlo simulations, and molecular dynamics simulations, to the burgeoning area of the hydrogen storage by metal–organic frameworks and covalent-organic frameworks. This review begins with an overview of the theoretical methods obtained from previous studies. Then strategies for the improvement of hydrogen storage in the porous materials are discussed in detail. The strategies include appropriate pore size, impregnation, catenation, open metal sites in metal oxide parts and within organic linker parts, doping of alkali elements onto organic linkers, substitution of metal oxide with lighter metals, functionalized organic linkers, and hydrogen spillover (186 references).

1. Introduction

Recently, the dramatic increase in the price of gasoline has activated research to find new energy sources. Of various renewable energy sources, hydrogen is very attractive due to its high power density of 33.3 kW h kg^{-1} (higher than methane at 13.9 kW h kg^{-1} and gasoline at 12.4 kW h kg^{-1}), abundance and non-polluting nature.[1] However the main concern to realize the hydrogen economy era is the efficient storage and transport of this highly flammable gas.[2] There are several methods toward hydrogen storage such as a high-pressure tank, cryogenic liquefaction of hydrogen, and adsorption in solid materials.[1]

The high-pressure tank would contain up to about 4% hydrogen by mass, however the fuel would be available at a pressure dropping from 450 bar to zero over-pressure, leading to additional pressure control technology.[1] Above all, the high-pressure compression is significantly dangerous. The cryogenic liquefaction of hydrogen is interesting from the point of view of high hydrogen mass per container volume. The density of liquid hydrogen is 70.8 kg m^{-3} (70.6 kg m^{-3} for solid hydrogen). However this technology has liquid boil-off problems in cryogenic systems.[1] On the other hand, adsorption in solid materials is safer than any other method for hydrogen storage and there are two strategies for the adsorption of hydrogen: dissociative adsorption (DA) and associated adsorption (AA) of hydrogen.[3]

Materials and Process Simulation Center (139-74), California Institute of Technology, Pasadena, California, 91125, USA. E-mail: wag@wag.caltech.edu; Fax: +1 626 585 0918; Tel: +1 626 395 2731
† Part of the metal–organic frameworks themed issue.
‡ Present address: Korea Research Institute of Standards and Science, Daejeon, Republic of Korea.

Sang Soo Han

Sang Soo Han was born in Korea, 1976. He obtained his PhD degree from Korea Advanced Institute of Science and Technology (KAIST), Korea in 2005, working with Prof. Hyuck Mo Lee. Then, from 2005–2009 he was a postdoctoral researcher with Prof. William A. Goddard III at California Institute of Technology, USA. Since February 2009, he has been a senior researcher at the Korea Research Institute of Standards and Science (KRISS), Korea. His research focuses on theoretical studies on hydrogen storage and CCS (carbon dioxide capture and storage) using metal–organic frameworks (MOFs).

José L. Mendoza-Cortés

José L. Mendoza-Cortés was born in Pochutla, Oaxaca, México in 1985. He learned about the physical sciences when he participated in the international chemistry olympiad at the age of 16. He received his BSc (2008) from Instituto Tecnológico y de Estudios Superiores de Monterrey (ITESM), Campus Monterrey, México. He has carried out research at University of Illinois Urbana-Champaign with Prof. Jeffrey S. Moore in 2006, at UCLA with Prof. Omar M. Yaghi in 2007–2008 and at the California Institute of Technology with Prof. William A. Goddard III from 2008 to present. He is currently a PhD student in Materials Science at Caltech.

DA is generally for solid metal hydrides in which, after surface adsorption, molecular hydrogen is dissociated into atoms that form a solid solution of a hydride phase.[1,3] Although metal hydrides show high hydrogen storage capacities at low pressure and high volumetric densities, they suffer from large barriers in dissociating the H–H bond to store the hydrogen and large barriers in recombining the H atoms to desorb H_2. Also, due to high binding energies for binding the hydrogen atoms to the metal hosts, one should manage the heat generated during the hydrogen charging/discharging process to apply the DA method into on-board vehicles. In contrast, AA binds the H_2 as a molecule by van der Waals interactions between the physisorbed H_2 molecules and the host material, and thus the binding energy is typically less than 10 kJ mol^{-1}.[4] This indicates that there are no problems with reversibility and large heat release on charging of hydrogen. However this low interaction energy means that adsorption of H_2 takes place only at low temperatures such as 77 K. But here the challenge has been to obtain sufficiently strong bonding to molecular H_2 to achieve the 2010 US DOE (Department of Energy) target of 6.0 wt% and 45 g L^{-1} near room temperature (−30 to 50 °C) with pressures $\leq$100 bar.[5]

Until now, hydrogen storage using AA has been studied mainly with porous materials that show large surface areas, such as zeolites,[6] carbon materials (activated carbon[7] and nanotube structures[8]), BN nanotubes,[9] and polymers.[10] However the evolution of new porous materials called metal–organic frameworks (MOFs) provides a new vision into the AA method where the MOFs are crystalline materials composed of metal oxide and organic units.[11,12]

The Yaghi group[13] first reported that a MOF (MOF-5) with a surface area of 3534 m^2 g^{-1}, where inorganic $[OZn_4]^{6+}$ groups are joined to an octahedral array of $[O_2C–C_6H_4–CO_2]^{2-}$ (1,4-benzenedicarboxylate, BDC) groups to form a porous cubic framework, showed 4.5 wt% H_2 uptake at 78 K and 0.8 bar and it stored 1 wt% of H_2 at 298 K and 20 bar. Although the H_2 uptake amount for MOF-5 at 77 K was reported again later as 1.30[14] wt% at 1.01 bar (1 atm) and 1.51[15] wt% at 1.13 bar, the result was still exciting enough to activate many researchers to study this topic. Representatively, Wong-Foy *et al.*[16] reported a high H_2 uptake amount of 7.0 wt% and 32 g L^{-1} at 77 K and 70 bar for MOF-177 with a surface area of 4746 m^2 g^{-1}, the framework consisting of tetrahedral $[OZn_4]^{6+}$ clusters linked by the tritopic linker BTB (1,3,5-benzenetribenzoate), and Dincã *et al.*[17] showed another MOF (surface area: 2100 m^2 g^{-1}) with 5.1 wt% and 43 g L^{-1} at 77 K and 45 bar, where the MOF has the formation of $[Mn(DMF)_6]_3[(Mn_4Cl)_3(BTT)_8(H_2O)_{12}]_2$·42DMF·11$H_2O$·20$CH_3OH$ with a cubic topology, where DMF = dimethylformamide and BTT = 1,3,5,-benzenetris-tetrazolate. As seen in these results, MOFs show higher reversible hydrogen uptake than any other porous materials.

Recently, the Yaghi group also synthesized two-dimensional[18,19] and three-dimensional[20,21] covalent organic frameworks (COFs) where the organic building units are held together by strong covalent bonds, such as C–C, C–O, B–O, and Si–C, rather than metal ions to produce the materials. The COFs have high surface areas (3472 m^2 g^{-1} for COF-102 and 4210 m^2 g^{-1} for COF-103) similar to MOFs, as well as showing very low crystal densities (0.17 g cm^{-3} for COF-108).[20] These characteristics make COFs excellent candidates for the storage of H_2.

In considering gas adsorption, one needs to distinguish excess adsorption and total (or absolute) adsorption.[22–25] When an adsorbate gas (*e.g.* H_2) is in contact with a solid adsorbent (*e.g.* MOFs), the region near the solid surface is called the adsorbed phase, which arises from the gas–solid intermolecular forces of attraction. This adsorbed phase may extend several diameters of the adsorbate molecules from the solid surface. However, the size and structure of the adsorbed phase and the actual density and composition profiles of the adsorbates within the adsorbed phase are generally quite difficult to characterize experimentally. Consequently, their properties are unknown functions of the bulk gas phase pressure and system temperature. Therefore, the experimentally observed mass change in the sample is represented as the difference between the total adsorbed amount and the bulk density of the adsorbate, which is expressed by a simple equation:[24,25]

$$N_{\text{total}} = N_{\text{excess}} + \rho_{\text{bulk}} V_{\text{pore}} \quad (1)$$

where N_{total} is the total adsorbed amount, N_{excess} is the excess amount, ρ_{bulk} is the bulk density of H_2, and V_{pore} is the pore volume of an adsorbent. Thus, most experimental measurements are reported as an excess adsorption amount. However, the 2010 DOE target[5] of 6.0 wt% and 45 g L^{-1} [1] is in terms of the total amount, leading to the importance of this quantity.

In using eqn (1), ρ_{bulk} is usually from the experimental NIST database[26] and is experimentally measured in a free volume. (Here note that the ρ_{bulk} is the bulk density.) However MOFs and COFs have pore sizes from 3.8 for IRMOF-5 to 28.8 Å for

William A. Goddard III

William A. Goddard III obtained his BS Engr. from UCLA in 1960 and his PhD in Engineering Science and Physics from California Institute of Technology (Caltech) in Oct. 1964. Since Nov. 1964, he has been a member of the Chemistry faculty at Caltech where he is now the Charles and Mary Ferkel Professor of Chemistry, Materials Science, and Applied Physics. His current research interests include: (1) new methodology for quantum chemistry, reactive force fields, molecular dynamics, mesoscale dynamics, statistical mechanics, electron dynamics; (2) applications of atomistic simulations to chemical, biological, and materials systems, including catalysis (homogenous and heterogeneous), polymers, semiconductors, superconductors, and metal alloys; (3) protein structure prediction (GPCRs), drug design, incorporation of non-natural amino acids; (4) applications of theory to industrial problems in catalysis, polymers, fuel cells, energetic materials, nanoelectronics, and batteries.

IRMOF-16.[27] Thus, the H_2 density in these confined volumes may be different from the ρ_{bulk},[28,29] making obtaining an accurate total amount by an experiment difficult. On the other hand, a computer simulation (*e.g.* grand canonical Monte-Carlo (GCMC)) could predict accurate H_2 density in the nanopores if one uses accurate force fields (FFs) between guest (H_2)–host (MOFs and COFs) and guest–guest, indicating that the theoretical method is very useful to obtain the total adsorption amount of H_2. Moreover, in a computer simulation one is easily able to build structural models of MOFs and COFs, which are very helpful to find new materials with higher hydrogen capacities. Due to these advantages of computer simulations, many researchers have been using these virtual experiments to investigate H_2 storage in MOFs and COFs.

Therefore, we will review here recent theoretical advances in H_2 storage in MOFs and COFs, and then in detail discuss ways to improve the H_2 storage inferred from the theoretical and experimental studies reported so far.

2. Recent computational studies on hydrogen storage in MOFs and COFs

Recent computational studies are largely divided into three methodologies: *ab initio* or density-functional theory (DFT) calculations to investigate binding energies of H_2 to MOFs and COFs, GCMC simulations to predict H_2 uptake amounts in them, and molecular dynamics (MD) simulations to investigate H_2 diffusion in them.

2.1 *Ab initio* and DFT calculations on H_2 adsorption in MOFs and COFs

After the Yaghi group[13] first reported the high H_2 uptake capacity of MOF-5 in 2003, Hüber *et al.*[30] most promptly investigated H_2 binding to the MOF using a theoretical approach. They focused on the interaction of H_2 with the aromatic systems C_6H_5X (X = H, F, OH, NH_2, CH_3, and CN), $C_{10}H_8$ (naphthalene and azulene), $C_{14}H_{10}$ (anthracene), $C_{24}H_{12}$ (coronene), *p*-$C_6H_4(COOH)_2$ (terephthalic acid), and *p*-$C_6H_4(COOLi)_2$ (dilithium terephthalate) using second-order Møller–Plesset (MP2)[31] calculations with the approximate resolution of the identity (RI-MP2)[32] in the TZVPP (triple-ξ valence basis[33] supplemented with the polarization functions of the cc-pVTZ basis[34]). The calculations show that H_2 binding energies to benzene and naphthalene are 3.91 and 4.28 kJ mol^{-1}, respectively, indicating that enlarging the aromatic system increases the interaction energy. In the same year (2004), similar works were reported by Sagara *et al.*[35] and Hamel and Côté.[36] Sagara *et al.*[35] calculated H_2 binding energies to H_2-1,4-benzenedicarboxylate-H_2, the organic linker part in MOF-5, as well as to the $Zn_4O(HCO_2)_6$ cluster, the metal oxide part in MOF-5, using the MP2 methodology and showed that the zinc oxide cluster has a higher H_2 binding energy than the organic linker part. And Hamel and Côté[36] calculated H_2 binding energy to benzene with *ab initio* methods such as MP2 and coupled cluster with noniterative triple excitation [CCSD(T)][37] as well as DFT methods of local-density approximation (LDA)[38] and generalized gradient approximation (GGA)[39] where they considered several H_2 configurations on the benzene. Also they calculated theoretical rotational spectra of the adsorbed H_2 and found that the theoretical result is comparable to the experimental inelastic neutron scattering (INS) spectra for H_2 adsorbed in MOFs.[13,27] In 2005, Sagara *et al.*[40,41] re-calculated H_2 binding energies for the organic linker part and Zn oxide part in MOF-5 (IRMOF-1) using MP2 with the quadruple zeta QZVPP[33,34] basis set, larger than the previous TZVPP,[35] in order to obtain more accurate H_2 binding energies. Also they calculated H_2 interactions with organic linkers in various MOFs (IRMOF-1,[27] IRMOF-3,[27] IRMOF-6,[27] IRMOF-8,[27] IRMOF-12,[27] IRMOF-14,[27] IRMOF-18,[14] and IRMOF-993) and found that the larger linkers showed the higher H_2 binding energies and were able to bind multiple hydrogen molecules per side, and the addition of an NH_2 or CH_3 group to each linker could provide up to a 33% increase in the binding energy.[40] After 2005, several MP2 or DFT works on H_2 interaction with organic linkers of MOFs were reported by Buda and Dunietz[42] (MP2 work), Lochan and Head-Gordon[43] (MP2), Negri and Saending[44] (MP2 and DFT), Klontzas *et al.*[45] (MP2 and DFT), Gao and Zeng[46] (MP2 and DFT), Lee *et al.*[47] (DFT), Han *et al.*[48] (MP2), Sagara and Ganz[49] (MP2), and Kuc *et al.*[50] (MP2). Especially, for the first time we considered H_2 binding with three different metal oxide clusters, namely $Zn_4O(HCO_2)_6$, $Mg_4O(HCO_2)_6$ and $Be_4O(HCO_2)_6$, in IRMOF types using MP2/QZVPP calculations, and found that the substitution of metal sites from Zn to Mg and Be does not change the basic configuration of the $M_4O(HCO_2)_6$ cluster and the Mg cluster has the strongest H_2 binding energy.[48]

With MP2 calculations, one is not able to consider periodic crystals at the current technical level. Instead, to calculate H_2 binding energies in MOF crystals, DFT calculations should be used. The DFT application to the MOF-5 crystal was tried by Mulder *et al.*,[51] and Mueller and Ceder.[52] Both papers showed that the strongest interactions with hydrogen are located near the Zn_4O clusters although they reported different H_2 binding energies to the Zn_4O clusters (70 meV per H_2 by Mulder *et al.*[51] and 20 meV per H_2 by Mueller and Ceder[52]), which is validated by some experimental[53–57] and theoretical[35,48,58] works. As shown so far, *ab initio* and DFT theories are very helpful to calculate H_2 binding energies to MOFs and then provide good information on the H_2 adsorption sites in MOFs.

Additionally, here we need to compare between the *ab initio* and DFT methods for the calculation of van der Waals interactions (*e.g.* H_2 interaction with MOFs and COFs). Because of the nature of van der Waals interactions (induced dipole–dipole), the wave function must at least include double excitations from a Slater determinant reference corresponding to single excitations of each subsystem. This means that *ab initio* methods used should be at least of the level of MP2 and CCSD. However, since DFT methods do not consider the excitation, they do not provide accurate long-range dispersion interactions.[59] In addition, it turns out that the triple excitations also have a very important contribution to the dispersion energy,[60] and then the CCSD(T) method would be more accurate in calculating van der Waals interactions than MP2, however MP2 has a greater advantage in aspect of calculation time.

2.2 GCMC simulations for prediction of H_2 uptake capacity in MOFs and COFs

GCMC simulation is a commonly used technique to study gas adsorption properties in confined and bulk fluids.[61] The simulation is conducted in a constant volume system defined by a simulation box, in which the number of fluid particles and configuration energy are allowed to fluctuate at constant temperature and chemical potential. Random microstates are generated based on the well-established Metropolis scheme,[62] involving four types of movements: creation, deletion, displacement and rotation of fluid particles. Also there is a case ignoring the rotation of fluid particles if the particle means a gas molecule itself, not an atom in the gas molecule. Since a hydrogen molecule H_2 has a linear conformation, the ignoring of rotation during the GCMC algorithm may lead to inaccuracy in the simulation (on the other hand, ignoring rotation in the case of CH_4 uptake would be fine because CH_4 has a spherical conformation). Also during GCMC simulation, it is assumed that structures of adsorbent materials (*e.g.* MOFs and COFs) are fixed.

A study on H_2 uptake in MOF-5 by GCMC simulation was first tried by Sagara *et al.*[35] in 2004 where they used the typical universal force field (UFF).[63] The GCMC simulation showed that a simulated H_2 loading curve up to 1 bar at 78 K was overestimated by 25% in comparison to an experimental result.[14] Yang and Zhong[64] simulated H_2 adsorption isotherms for IRMOF-1, IRMOF-8, and IRMOF-18 using GCMC and the OPLS force field (OPLS-AA)[65] where they showed better results for IRMOF-1 and IRMOF-18 than Sagara *et al.*[35] Garberoglio *et al.*[66] calculated H_2 adsorption isotherms for various MOFs (MOF-2,[67] MOF-3,[68] IRMOF-1,[27] IRMOF-6,[27] IRMOF-8,[27] and IRMOF-14[27]) with the UFF[63] and DREIDING.[69] Their simulations overestimated H_2 uptake of IRMOF-1, while underestimated H_2 uptake of IRMOF-8 up to 1 bar at 77 K, although the H_2 uptake of IRMOF-1 showed better agreement with an experiment through quantum effect correction[70] of the hydrogen molecules. However the simulation reported the important fact that at room temperature all MOFs considered were not able to meet the DOE target.

Similarly, Yang and Zhong[71] simulated H_2 isotherms at 298 K up to 7 MPa (70 bar) for IRMOF-1 and Cu-BTC (also known as HKUST-1)[72] using the OPLS-AA FF[63] with additional refinement in the work and showed their simulation was in good agreement with experiments.[73] They also extended their simulation technique into MOF-505[74] with open metal sites,[75] and found that the open metal sites have a favorable impact on the H_2 adsorption in MOFs, however the MOF still showed low H_2 uptake at room temperature.[75]

Frost *et al.*[76] clarified the effects of surface area, free volume, and heat of adsorption on H_2 uptake in MOFs by GCMC simulation with the DREIDING FF[69] although their simulation tended to underestimate up to 1 bar and overestimate from the pressure owing to use of the empirical FF. They revealed the existence of three adsorption regimes: at low pressure (0.1 bar), hydrogen uptake correlates with the heat of adsorption; at intermediate pressure (30 bar), uptake correlates with the surface area; and at the highest pressure (100 bar), uptake correlates with the free volume.

Jung *et al.*[77] studied the effect of catenation on hydrogen adsorption onto the interpenetrating MOFs using the GCMC and UFF,[63] and showed that the small pores generated by catenation can play a role to confine the hydrogen molecules more densely, so that the capacity of interpenetrating MOFs could be higher than that of the non-interpenetrating MOFs. Recently a similar work on the effect of catenation on H_2 uptake in MOFs was also reported by Ryan *et al.*[78] where they used the DREIDING FF[69] during GCMC simulations. According to the simulation,[78] catenation can be beneficial for improving hydrogen storage in MOFs at cryogenic temperatures and low pressures, however not necessarily at room temperature.

Recently, the GCMC simulation has been applied to new MOFs which were experimentally synthesized. Liu *et al.*[79] synthesized a new MOF material, $[Zn(bdc)(ted)_{0.5}]$ (bdc = benzenedicarboxylate, ted = triethylenediamine), and showed good agreement between experimental and simulational H_2 uptake isotherms at 77 and 298 K where they used the UFF[63] and DREIDING[69] together with the quantum effect correction.[70] However, they (Liu *et al.*)[80] also applied the same simulational technique to the Cu-BTC[72] MOF (the activation process of the sample was experimentally improved in the work) and showed a slight disagreement between simulations and experiments for the H_2 adsorption isotherm at 77 K. And Noguchi *et al.*[81] synthesized a new Cu-based MOF $[Cu(4,4'\text{-bipyridine})_2(CF_3SO_3)_2]_n$ of one-dimensional pore networks. They measured H_2 and D_2 adsorption isotherms of the MOF at 40 and 70 K and then compared them with GCMC simulated isotherms where the OPLS-AA was used. Their simulation showed a tendency to slightly overestimate H_2 and D_2 adsorption isotherms although quantum effect was considered.

Some research groups studied imaginary MOFs (not synthesized yet) for improved design to increase H_2 storage capacity through GCMC simulations. Zhang *et al.*[82] designed five new MOF materials by exchanging the organic linker (BDC) of MOF-5, where BDC was replaced with oxalate and with new organic linkers by introducing –F, –Cl, $–CF_3$, and $–CCl_3$ to tone up the electronegativity of linkers. Then they simulated their H_2 adsorption isotherms up to 1 bar at 77 K using the DREIDING[69] FF and found that the proposed MOFs showed much higher H_2 uptake behavior at low pressure (up to 1 bar).[82] Since the current MOFs show very low H_2 uptake amount at room temperature, Frost and Snurr[83] investigated how much the heat of adsorption should be increased to meet the current DOE target by artificially increasing the hydrogen–MOF Lennard-Jones attraction with GCMC simulations. They found that if MOF materials can achieve an isosteric heat of 10–15 kJ mol^{-1} with a free volume between 1.6 and 2.4 $cm^3\ g^{-1}$, gravimetric H_2 uptake of 6% could be achieved, and MOFs with free volumes less than 1.5 $cm^3\ g^{-1}$ or void fractions of less than 75% will need isosteric heats larger than 20 kJ mol^{-1} to achieve 6 wt% and 30 g cm^{-3} of H_2.[83]

GCMC simulation work on H_2 uptake in COF systems was first reported by Giovanni Garberoglio in 2007.[84] He simulated H_2 adsorption isotherms for 3-dimensional COFs (COF-102, COF-103, COF-105, and COF-108) at 77 and

298 K using UFF[63] and DREIDING,[69] and showed that the best COF is COF-105 (maximum H_2 uptake of ~10.5 wt%) at 77 K and COF-108 (maximum H_2 uptake of ~0.9 wt%) at 298 K. Another similar work was reported by Klontzas *et al.*[85] Using an empirical Lennard-Jones potential,[86] they predicted that the gravimetric uptake for COF-108 reaches a value of 21 wt% at 77 K and 100 bar and 4.5 wt% at room temperature and 100 bar.[85] GCMC simulation work on H_2 uptake in 2-dimensional COFs (COF-6, COF-8, and COF-10)[19] was performed with the DREIDING[69] FF by Garberoglio and Vallauri.[87]

Most GCMC works introduced above so far used empirical FFs such as UFF,[63] DREIDING,[69] and OPLS-AA,[65] where the UFF[63] and DREIDING[69] were developed by our group. All of the three FFs were developed for predicting structures and dynamics of organic, biological, and main-group inorganic molecules, mainly for covalent bonds between atoms. Thus they would predict rough binding energies for non-bonded interactions between H_2 and MOFs, so that combination of the GCMC simulation and the FFs might provide inaccurate H_2 uptake in MOFs and COFs. In the previous GCMC studies the hydrogen molecule is treated as a diatomic molecule modeled by a Lennard-Jones potential developed from Buch[88] or Darkrim and Levesque.[89]

However we developed accurate non-bonded FFs for H_2--MOFs[48,90] (or COFs)[91] and H_2--H_2[92] from high level *ab initio* calculations where all of our FFs describe interactions between atoms. From the *ab initio* based FFs, we showed accurate H_2 adsorption isotherms for cubic[48] and hexagonal[90] crystalline IRMOFs, and 2D-[91] and 3D-COFs.[91] For example, our simulations[48] for IRMOF-1 indicate 1.28 wt% at 77 K and 1 bar, close to an experimental result[14] of 1.30 wt% under the same conditions, and show 4.17 and 4.89 wt% at pressures of 20 and 50 bar and 77K, which are also comparable to the experimental results[16] of 4.5 and 4.9 wt% under the same conditions. On the other hand, previous GCMC simulations with empirical FFs for IRMOF-1 at 77 K and 1 bar showed 1.62 wt% by Sagara *et al.*,[35] 1.33 wt% by Yang and Zhong,[64] 1.38 wt% by Garberoglio *et al.*,[66] 1.33 wt% by Frost *et al.*,[76] and 1.27 wt% by Zhang *et al.*,[58] which are similar to our simulation except for Sagara *et al.*[35] However at 77 K and pressures of 20 and 50 bar, Yang and Zhong[64] showed ~6.5 and ~8.0 wt%, Garberoglio *et al.*[66] showed ~6.3 and ~7.0 wt%, and Frost *et al.*[76] showed ~7.8 wt% and ~8.7 wt%, respectively, which are overestimated in comparison to the experimental values.[16] Such overestimation is more pronounced as pressures increase. Our simulation technique reproduces well H_2 adsorption isotherms for hexagonal MOF-177[93] at 77 K in which an experiment[16] exhibits the maximum H_2 uptake of 7.0 wt% at 70 bar, very similar to our simulation result (7.1 wt% at 80 bar).[90] We also simulated H_2 adsorption isotherms of COFs and then compared them with an experiment.[91] For COF-5, our simulation is in excellent agreement with an experiment (3.3 *vs.* 3.4 wt% at 50 bar) performed in the work.[91] Recently we have also developed *ab initio* based FFs for calculation of CH_4 uptake in COFs and found that our FFs do reproduce well experimental CH_4 adsorption isotherms.[94] As shown so far, the *ab initio* based GCMC simulation can provide more accurate H_2 adsorption isotherms than simulations with empirical FFs. In addition, differently from previous GCMC works, we do not use the NIST database[26] for ρ_{bulk} in eqn (1) in calculating the excess H_2 uptake amount. The Gibbs surface excess is the absolute amount of gas contained in the pores minus the amount of gas ($\rho_{bulk}V_{pore}$ in eqn (1)) that would be present in the pores in the absence of gas–solid intermolecular forces.[95] In calculating the $\rho_{bulk}V_{pore}$, we turn off all the attractive interaction parts between the H_2 and MOFs (or COFs) in our developed FFs (while H_2–H_2 interaction terms are used as is) and then perform additional GCMC simulations at each temperature and pressure. This fact means that our simulation technique for the calculation of the H_2 uptake amount does not use any experimental information (except crystal information) to calculate the H_2 uptake amount, thus it is a pure theoretical approach.

2.3 MD simulations on H_2 diffusion in MOFs and COFs

For practical hydrogen storage media, the kinetic properties of hydrogen are also very important together with high hydrogen uptake capacity. To investigate the kinetic properties such as diffusion of H_2 in MOFs or COFs, MD simulation is appropriate.

The first MD simulation on the diffusion of H_2 molecules in MOFs was reported by Yang and Zhong[64] where they calculated the self-diffusivity of H_2 in IRMOF-1, -8, and -18 as a function of pressure at 77 K. The simulation indicated that the diffusion of H_2 in IRMOF-18 is much lower than diffusion in the other two MOFs due to the steric hindrance effects of the pendant CH_3 groups in IRMOF-18, and H_2 molecules diffuse more rapidly in IRMOF-8 than in IRMOF-1 because of the relatively larger pore size of IRMOF-8. The second MD simulation on H_2 diffusion in IRMOF-1 was reported by Skoulidas and Sholl[96] where the simulation was performed at room temperature. They calculated the self-diffusivity and transport diffusivity of H_2 adsorbed in the MOF as a function of H_2 loading (pressure), and found that the self-diffusivity of H_2 in IRMOF-1 decreases as the loading is increased while the transport diffusivity increases monotonically.

Here, the self-diffusivity describes the diffusive motion of a single particle (H_2) and the transport diffusivity indicates the transport of mass and the decay of density fluctuations in the system.[97] In general, the self-diffusivity is theoretically measured under equilibrium MD simulation, while the transport diffusivity is measured under non-equilibrium MD simulation conditions in which finite concentration gradients exist.[97]

In 2008, some research groups reported H_2 diffusion in various MOFs using MD simulations. Liu *et al.*[98] calculated the self-diffusivity of H_2 in ten different IRMOFs with and without interpenetration (catenation) and showed that catenation can reduce H_2 diffusivity by a factor of 2 to 3 at room temperature as well as the bigger free volume leads to a larger H_2 diffusivity. Keskin *et al.*[99] investigated the self-diffusivity of H_2 in Cu-BTC[72] MOF. Liu *et al.*[79] calculated the self-diffusivity and transport diffusivity of H_2 in the [Zn(bdc)(ted)$_{0.5}$] MOF synthesized in the work and found that the diffusivities of H_2 in the MOF are comparable to H_2 in IRMOF-1 at 298 K. And Salles *et al.*[100] calculated the self-diffusivity of H_2

in two MOFs, MIL-47(V)[101] and MIL-53(Cr),[102] and showed that the hydrogen diffusivity at low loading is about 2 orders of magnitude higher than in zeolites, which was also first supported by the quasielastic neutron scattering experiment. They also applied the simulational and experimental methods to CH_4 diffusion in the same MOFs.[103]

A MD simulation study on H_2 diffusion in COFs was first tried by Garberoglio and Vallauri.[87] They calculated the self- and transport diffusivities of H_2 in 2D-COFs (COF-6, COF-8 and COF-10)[19] and showed that H_2 diffusion in the COFs is one order of magnitude more rapid than in MOFs. As far as we know, the H_2 diffusivity in 3D-COFs has not been reported yet.

All the MD simulation studies reviewed above are on H_2 diffusion inside MOFs or COFs. Studies on the interfacial region between the gas phase of H_2 and MOFs (or COFs) have not been reported yet although it would also provide useful information to understand the real kinetics of H_2. This could be a good theoretical topic for future works. Moreover, all of the MD works used empirical FFs such as UFF[63] and DREIDING[69] during the MD simulation, thus we expect that the accuracy of the MD simulation could be improved by using our *ab initio* based FFs.[48,90–92]

2.4 FFs for prediction of crystal structures of MOFs and COFs

To date, most experimental and theoretical research groups have used the standard UFF[63] and DREIDING[69] to build or predict crystal structures of MOFs and COFs. The FFs have provided reasonable crystal information, comparing with experimental X-ray diffractions, and have reproduced well peculiar properties of MOFs such as negative thermal expansion.[53,104–106]

On the other hand, studies on FF development for providing accurate crystal structures of MOFs and COFs were recently performed by Tafipolsky *et al.*,[107] Huang *et al.*,[108] Greathouse and Allendorf,[109] and Schmid and Tafipolsky.[110] Tafipolsky *et al.*[107] developed a new MM3[111] FF for IRMOF-1 from DFT and *ab initio* calculations. The FF predicts the IRMOF-1 structure successfully and yields vibrational frequencies in reasonable agreement with the predictions of DFT. It is also encouraging that the self-diffusivity of a benzene obtained from MD simulation with the FF is within ~30% of the value measured by NMR.[112] Huang *et al.*[108] developed a FF from DFT calculations and experimental data and then calculated the phonon thermal conductivity and vibrational power spectra of IRMOF-1. Greathouse and Allendorf[109] modified the original CVFF[113] for IRMOF-1 with previous DFT and experimental results on the negative thermal expansion property, elastic moduli, and vibrational power spectra. And Schmid and Tafipolsky[110] developed a FF for COF-102 and the FF was validated with DFT results on crystal information and vibrational modes of COF-102.

3. Strategies for improved designs of MOFs and COFs with high hydrogen storage capacity

In 2005, Rowsell and Yaghi[114] systematically discussed six strategies (high porosity with appropriate pore size, impregnation, catenation, open metal sites, MOFs with light metals, and functionalized linkers) for high hydrogen adsorption in MOFs. The paper opened a new window for improved hydrogen storage in MOFs (and COFs), and since then many developments have been reported with help of the paper. Thus, in this review we will update and extend the strategies mentioned in the paper[114] and additionally introduce some new strategies.

3.1 Appropriate pore size

As soon as the possibility of MOFs as a hydrogen storage medium was reported,[13] many scientists have focused on the relationship between pore size (or surface area) of the MOFs and H_2 storage amount, and they have shown that the gravimetric H_2 storage amount is linearly proportional to the pore size (or surface area).[15,16,48,73,76,90,115–123]

Lin *et al.*[117] synthesized three MOFs with NbO-type topologies using $[Cu_2(O_2CR)_4]$ paddle-wheel units and biphenyl-3,3′,5,5′-tetracarboxylic acid, terphenyl-3,3″,5,5″-tetracarboxylic acid, and quaterphenyl-3,3‴,5,5‴-tetracarboxylic acid and then investigated H_2 adsorption behaviors as a function of their pore volume. They found the maximum amount of H_2 adsorbed increased with increasing pore size, while the maximum adsorbate density decreased with increasing pore size, indicating that the contrasting adsorbed H_2 density with increasing pore size suggests that an optimum pore size exists. Therefore it was concluded that a strategy of only increasing pore volume may not give the optimum hydrogen storage material.

Also, we studied the effect of pore volume on the H_2 storage amount in cubic crystalline IRMOFs (Fig. 1) using GCMC simulation with *ab initio* based FFs.[48] Fig. 2 shows total and excess H_2 uptake for the five MOFs (shown in Fig. 1) in gravimetric and volumetric units at 77 K and 300 K.[48] At 77 K, gravimetric H_2 uptake (Fig. 2(a)) increases with increasing organic linker size (pore size). For example, at 77 K and 100 bar MOF-C6 (IRMOF-1) has an excess H_2 uptake of 5.09 wt% (total uptake: 6.46 wt%), MOF-C10 (IRMOF-8) has an excess uptake of 5.69 wt% (total uptake: 7.52 wt%),

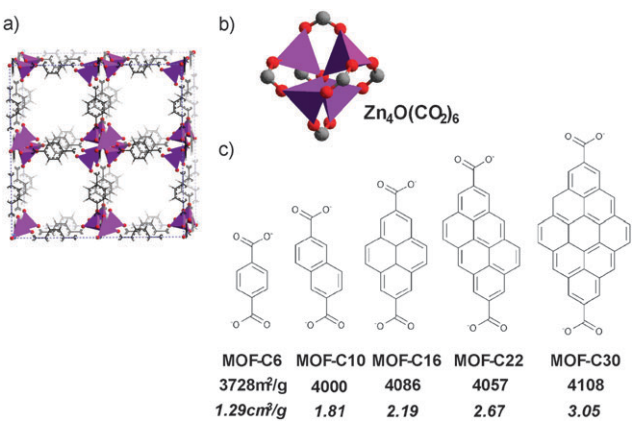

Fig. 1 Atomistic structures of MOFs. An overview of the complete structure is shown in (a). Here, the purple tetrahedra correspond to the metallic nodes in (b), and the different linkers are shown in (c). MOF-C6 is same as the well-known MOF-5 (or IRMOF-1), MOF-C10 is IRMOF-8, and MOF-C16 is IRMOF-14.

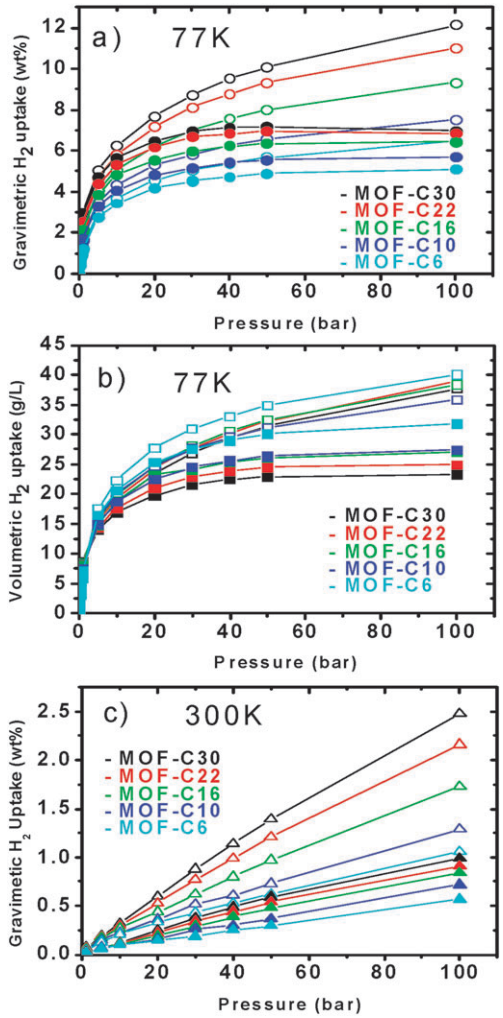

Fig. 2 Predicted H_2 adsorption isotherms for the five MOF systems shown in Fig. 1. (a) Gravimetric H_2 uptake at 77 K, (b) volumetric H_2 uptake at 77 K, and (c) gravimetric H_2 uptake at 300 K. Here, solid symbols indicate the excess uptake amount, and open symbols indicate the total uptake amount. Color codes are cyan = MOF-C6, blue = MOF-C10, green = MOF-C16, red = MOF-C22, and black = MOF-C30.

MOF-C16 (IRMOF-14) has an excess uptake of 6.43 wt% (total uptake: 9.32 wt%), MOF-C22 has an excess uptake of 6.84 wt% (total uptake: 11.02 wt%), and MOF-C30 has an excess uptake of 6.98 wt% (total uptake: 12.13 wt%). However volumetric H_2 uptake (Fig. 2(b)) generally decreases with increasing pore size, so that the best MOF in the volumetric unit is MOF-C6 with the smallest pore size. As shown here, gravimetric H_2 uptake is linearly proportional to the pore size of the MOFs, while volumetric uptake is generally inversely proportional to the pore size. For practical hydrogen storage materials, volumetric H_2 uptake capacity is a very important factor together with gravimetric uptake.[1] Thus similar to Lin *et al.*,[117] increasing the pore volume is not the only factor to be considered in the design of hydrogen storage materials. And the conclusion is also supported by Fig. 2(c) where the maximum gravimetric excess H_2 uptake at 300 K is near 1.0 wt% at 100 bar although total H_2 uptake is up to 2.5 wt% at this pressure. This result indicates that one might not be able to approach the DOE target by only increasing the pore size.

Similarly we also investigated the relationship between H_2 uptake and pore volume of MOFs with hexagonal structures using GCMC simulation, and obtained a similar conclusion.[90]

Some research groups have studied the optimum pore size for graphite using *ab initio* or DFT calculations, and all of them reached the same conclusion that the H_2 binding energy is maximized up to -13.0 kJ mol^{-1} with an interlayer distance of 6 Å.[124–127] (Here the 6 Å is just an interlayer distance of graphite, meaning a value obtained by ignoring van der Waals radii of carbon atoms in graphite. When considering the van der Waals radius, the pore size is close to the kinetic diameter (2.89 Å) of H_2 since the maximal attraction of an adsorbate would occur at a size the same as the diameter of the adsorbate.) The magic number (6 Å) is applicable to MOFs or COFs because their organic linkers consist of aromatic carbon rings (*e.g.* benzene) and the H_2 interaction with the carbon rings is similar with graphene.

Of current MOFs and COFs, COF-1 representatively has a pore size near the magic number. Since COF-1 has a graphite-like structure with an '*ABAB*' stacking layer sequence,[18] its pore size is two times that of one layer distance, leading to 6.7 Å (2 × 3.35 Å), as shown in Fig. 3. According to our previous GCMC simulation with *ab initio* based FFs, COF-1 has a very high heat of adsorption for H_2 (8.8 kJ mol^{-1}) due to the appropriate pore size, leading to exceptional H_2 uptake capacity at low pressure (1.7 wt% at 0.1 bar) which is much higher than other COFs (COF-5, COF-102, COF-103, COF-105, and COF-108). Also, COF-1 shows the highest volumetric uptake up to 20 bar among the COFs considered in the work and a peculiar H_2 adsorption behavior so that the ratio of excess H_2 uptake to total H_2 uptake at 100 bar is 0.99.

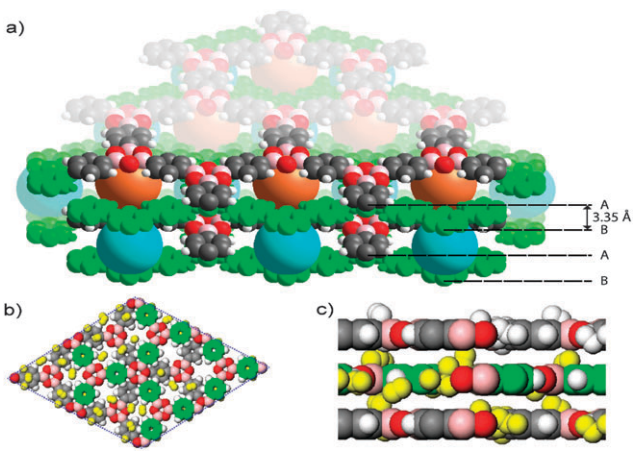

Fig. 3 (a) A unit cell of a COF-1 crystal with *ABAB* stacking layer sequences, where gray, pink, red, and white atoms correspond to carbon, boron, oxygen, and hydrogen atoms, as well as bronze and cyan balls indicating pores generated by the *AA* layers and *BB* layers, respectively. Top (b) and side (c) views of the COF-1 structure including adsorbed H_2 molecules (yellow), where gray atoms indicate carbon on an *A* layer and green atoms indicates carbon atoms on a *B* layer. The adsorbed H_2 molecules are sandwiched by two layers, leading to high H_2 binding energy.

However, at 300 K, COF-1 still shows a low H_2 storage amount (total 0.78 wt% and excess 0.75 wt% at 100 bar). To achieve a high adsorption of H_2 at room temperature and moderate pressures, the heat of adsorption should be in the range of 20–30 kJ mol^{-1},[114] higher than that (8.8 kJ mol^{-1}) in COF-1.

3.2 Impregnation

To make effective pore sizes in MOFs for high adsorption of H_2, Yaghi and co-workers[114] suggested the insertion of another adsorbate surface within large-pore MOFs. For example, they experimentally proved that large molecules such as C_{60} and Reichardt's dye can be included into MOF-177 from the solution phase,[93] and suggested that the impregnation with such inclusion could provide the more attractive sites that are ultimately necessary to improve H_2 uptake.[114] Nevertheless, as far as we know, no studies on the impregnation have been reported yet. Thus we investigated the effect of the C_{60} inclusion in MOF-177 on H_2 uptake using GCMC simulation.

Fig. 4 shows the C_{60}@MOF-177 structures obtained from our GCMC simulation at 300 K and 1 bar with the standard DREIDING[69] FF, in which MOF-177 can absorb sixteen C_{60} molecules in the unit cell under these conditions. And the C_{60} inclusion leads to a decrease in the free volume of the MOF to 0.61 $cm^3\ g^{-1}$ from 1.54 $cm^3\ g^{-1}$ for pure MOF-177.

From the C_{60}@MOF-177 structure of Fig. 4, we simulated H_2 adsorption isotherms at 77 K and 300 K with our *ab initio* based FFs,[48,90–92] and then compared them with those of MOF-177, shown in Fig. 5. The inclusion of C_{60} into MOF-177 increases H_2 uptake at low pressure compared with pure MOF-177 at 77 and 300 K. However due to the lower pore size of C_{60}@MOF-177, the H_2 storage capacity at high pressure is lower than MOF-177. We desired that the C_{60} inclusion would be positioned near the center of the pores in MOF-177 to minimize dead volumes for H_2 storage. However since the C_{60} attractively interacts with MOF-177 and another C_{60}, it could block the existing adsorptive sites on the MOF-177 (although it also provides additional adsorptive sites on C_{60}). At 300 K, the C_{60} inclusion slightly improves the H_2 uptake of MOF-177, nevertheless the uptake amount is still much lower than the DOE target of 6.0 wt%, indicating that impregnation might not be an effective alternative for practical hydrogen storage. In addition, it is noticeable that C_{60}@MOF-177 shows a smaller gap between total and excess H_2 uptake than MOF-177.

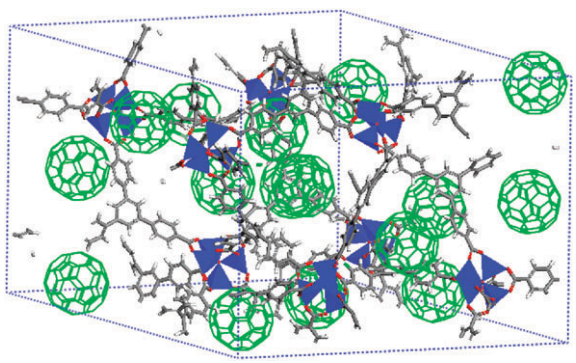

Fig. 4 A C_{60}-impregnated MOF-177 structure. This structure was obtained from a GCMC simulation on C_{60} uptake in MOF-177 at 298 K and 1 bar.

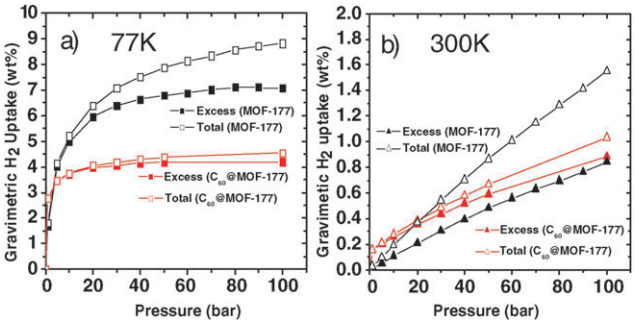

Fig. 5 Predicted H_2 adsorption isotherms for the C_{60}@MOF-177 structure (shown in Fig. 4) at 77 (a) and 300 K (b). Here, solid and open symbols indicate excess and total H_2 uptake, respectively. During GCMC simulations, one finds H_2 molecules inside C_{60}. However since H_2 molecules cannot diffuse into the perfect C_{60},[128] we ignore the H_2 molecules inside C_{60} in calculating H_2 uptake amounts.

3.3 Catenation

Framework catenation is another way to tune the pore size of MOFs.[129] Catenation is divided into two types: interpenetration[130] and interweaving (Fig. 6).[131] Interpenetration is that the frameworks are maximally displaced from each other by shifting the second framework exactly one half of the pore size in the *x*, *y*, and *z* directions; the interwoven MOFs minimize the distance between both frameworks without atomic overlap.[114]

Kesanli *et al.*[132] experimentally showed a high H_2 adsorption amount (1.12 wt% at 48 bar) at room temperature with interpenetrated MOFs, Sun *et al.*[133] synthesized interwoven MOFs showing a high H_2 uptake of 1.90 wt% at 77 K and 1 bar, and Rowsell and Yaghi[134] measured H_2 storage capacities of various MOFs and then found that catenated MOFs show the highest H_2 uptake at low pressure below 1 bar. After the results, some experimental studies[135–138] on H_2 uptake in catenated MOFs were reported.

The theoretical study on H_2 uptake in interpenetrated MOFs (IRMOF-9, -11, and -13) was first reported by Jung *et al.*[77] using GCMC simulations at 77 K. The simulation shows that the small pores generated by the catenation play a role in confining the H_2 molecules more densely, indicating

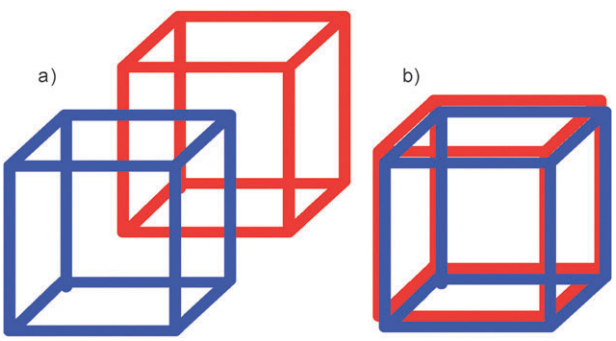

Fig. 6 Catenation of two MOFs: (a) interpenetration, and (b) interweaving.

that the interpenetrated MOFs have higher H_2 uptake than the non-interpenetrated MOFs at low pressure. However due to the small pores caused by the catenation the interpenetrated MOFs have lower H_2 uptake at high pressure. They also clarified the binding sites of H_2 in the interpenetrated MOFs where the adsorption sites with the largest binding energies are located in the very small volume surrounded by two zinc oxo clusters (metal–metal sites), the adsorption sites with the second largest binding energies are the metal–linker sites confined by a zinc oxo cluster of one chain and an organic linker of the other framework, and the adsorption sites with the lowest binding energies are the linker–linker sites, occupying the largest portion in the interpenetrated MOFs.

Ryan *et al.*[78] investigated H_2 uptake in both interpenetrated and interwoven MOFs (IRMOF-1, -10, and -16) at 77 and 298 K by GCMC simulations. Similar to Jung *et al.*,[77] they showed that at low pressures catenation is clearly beneficial for H_2 uptake, but at high pressures non-catenated MOFs exhibit higher H_2 uptake than their catenated MOFs. Their simulation for 298 K showed that in a gravimetric H_2 uptake unit the loading for the catenated structures is approximately one half that of the non-catenated structures, while in a volumetric unit a similar H_2 uptake amount is shown for catenated and non-catenated MOFs.

From the two simulational works,[77,78] we can conclude that catenation is helpful for H_2 uptake in MOFs at 77 K and low pressures, but it could not be at room temperature.

3.4 Open metal sites in the metal oxide parts of MOFs

So far, we have discussed improvement in H_2 uptake in MOFs through control of pore size. However the H_2 storage capacity is also improved using open metal sites in MOFs leading to stronger H_2 binding.

According to G. J. Kubas,[139] the d orbitals of a transition metal (M) interact with antibonding orbitals of a hydrogen molecule, leading to energetic stabilization of the M–H_2 bond. The transition metal–hydrogen complexes (M–H_2) can reversibly bind H_2 and the binding energy of H_2 to the transition metal can be varied between 20–160 kJ mol^{-1},[139] which is around the appropriate heat of adsorption range (20–30 kJ mol^{-1})[114] for high H_2 uptake at room temperature. Currently, the Kubas binding has been applied to enhance H_2 binding with open metal (transition metal) sites in MOFs.

There are many experimental studies reporting high binding energies using the open metal sites of MOFs.[17,74,140–153] Forster *et al.*[140,143] synthesized MOFs with exposed Ni^{2+} sites and the MOFs have high enthalpies of adsorption (9.4–10.4 kJ mol^{-1}). Yaghi and co-workers reported MOF-505 with open sites of Cu^{2+} where the MOF shows a high H_2 uptake amount of 2.5 wt% at 77 K and 1 bar.[74] Long and co-workers[17] synthesized a MOF with exposed Mn^{2+} sites and the MOF has a maximum heat of adsorption of 10.1 kJ mol^{-1}. Long and co-worker also experimentally exchanged the guest Mn^{2+} ion in $Mn_3[(Mn_4Cl)_3(BTT)_8(CH_3OH)_{10}]_2$ (BTT = 1,3,5-benzenetristetrazolate) MOF with Li^+, Cu^+, Fe^{2+}, Co^{2+}, Ni^{2+}, Cu^{2+}, and Zn^{2+} where the metals are unsaturated, and then investigated their H_2 uptake behaviors.[146] The new MOFs exhibited high H_2 storage capacities ranging from 2.00 to 2.29 wt% at 77 K and 900 torr, and the Co^{2+}-exchanged MOF showed an initial enthalpy of adsorption of 10.5 kJ mol^{-1}.[146] Zhou and co-worker[142] synthesized a new MOF (PCN-9) with $Co_4O(carboxylate)_4$ secondary building units similar to the active center of hemoglobin (open) and the MOF has a heat of adsorption of 10.1 kJ mol^{-1} showing a H_2 uptake of 1.53 wt% at 77 K and 1 bar. Similarly they also recently reported PCN-12 with open Cu sites where the MOF shows the highest H_2 uptake (3.05 wt%) at 77 K and 1 bar.[148] And, Vitillo *et al.*[150] reported a MOF (called CPO-27-Ni) with an initial heat of adsorption of −13.5 kJ mol^{-1}, the highest yet observed for a MOF where the CPO-27-Ni has open Ni^{2+} sites and a similar crystal structure to the typical MOF-74.[154] Recently Dincã and Long[153] reviewed in detail experimental H_2 uptake in MOFs with exposed metal sites. The exposed metal sites must increase the heat of adsorption of H_2, and then lead to an increase in H_2 uptake amounts at 77 K and low pressures (*e.g.* 1 bar), however there are no reports on H_2 uptake behavior at room temperature. Since the heat of adsorption is lower than the appropriate H_2 binding energy (20–30 kJ mol^{-1})[114] for high uptake around room temperature, we think that the current MOFs mentioned above might still have low H_2 uptake amounts at room temperature although they would show higher H_2 uptake at room temperature than other MOFs without open metal sites.

A theoretical study on these open metal sites of MOFs was first reported by Yang and Zhong.[75] They investigated H_2 adsorption sites in MOF-505[74] by GCMC simulation and DFT calculations where they reported a H_2 binding energy of −13.4 kJ mol^{-1} to the open metal site in the MOF. Also they predicted that the MOF has a low H_2 storage capacity at room temperature (*e.g.* 0.82 wt% at 298 K and 50 bar). Also, Kosa *et al.*[155] calculated H_2 binding energies to exposed Ni^{2+} and Mg^{2+} sites using DFT calculations where the exposed M^{2+} coordinated sites were modelled by neutral square pyramidal clusters, $ML_3L'_2$ with L = CH_3OCH_3 and L′ = OCH_3^-. In the work, they showed that the Ni^{2+} site has stronger H_2 binding energies (6 to 23 kJ mol^{-1}) than the Mg^{2+} site (∼1 kJ mol^{-1}).

Sun *et al.*[156] clarified the characteristics of H_2 binding to exposed Mn^{2+} sites in a MOF synthesized by Long and co-workers[17] through DFT calculations. As shown in Fig. 7, the H_2 binding to the exposed metal site results from the

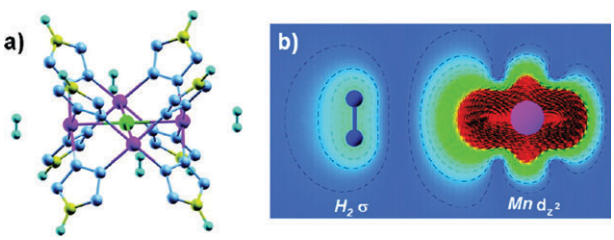

Fig. 7 (a) Simulative model for Mn-based MOF systems. The magenta, gray, yellow, green, and cyan balls represent Mn, N, C, Cl, and H atoms, respectively. Four H_2 molecules are adsorbed on the four Mn centers in the side-on configuration. (b) Electron density plot of an antibonding state between the H_2 σ and Mn d_{z^2} orbitals. Reproduced from ref. 156.

coupling between the H_2 σ and Mn d_{z^2} orbitals. They also replaced the Mn element in the original MOFs with early transition metals (Sc, Ti, V, and Cr) and calculated H_2 binding energies. The H_2 binding energies are 21.9 kJ mol^{-1} to Sc-MOF, 34.6 kJ mol^{-1} to Ti-MOF, 46.5 kJ mol^{-1} to V-MOF, 10.4 kJ mol^{-1} to Cr-MOF, and 8.4 kJ mol^{-1} to Mn-MOF (the experimental binding energy for Mn-MOF is 10.1 kJ mol^{-1}),[17] indicating that the binding energy to H_2 can be tuned from about 10 to 50 kJ mol^{-1} by using different transition metals in MOF systems.

3.5 Open metal sites in the organic linker parts of MOFs (or COFs)

According to our GCMC study,[48] although the metal-oxide cluster in MOFs is preferentially responsible for the H_2 adsorption at low pressure (H_2 loading), the importance of the organic linker is more and more enhanced with increased H_2 loading. For example, at 77 K and 30 bar, the organic linker accounts for 74% of the H_2 loading for MOF-5.[48] Similarly, for the MOFs with exposed metal sites in metal building units (mentioned in section 3.4), the proportion of metal building units is lower than that of the organic linker parts, and so at high pressure (generally the maximum H_2 uptake capacity is observed) organic linker parts would be more important than the metal building units. Therefore, to improve the maximum H_2 uptake amount of MOFs with high heats of adsorption of H_2, it is more interesting to make open metal sites within the organic linker parts of the MOFs.

The trial was recently performed by Kaye and Long.[157] They synthesized the MOF-5 with Cr metal centers attached to the benzene rings in an η^6 fashion through the chemical reactions of MOF-5, $Cr(CO)_6$, dibutyl ether, and THF. Also they measured the H_2 adsorption amount in the MOF-5 with the Cr metal centers at 298 K, however the adsorption amount is fewer than 0.2 molecules per formula unit.

After the experimental findings,[157] Lochan *et al.*[158] investigated interactions between H_2 molecules and the model of exposed Cr metal sites (half-sandwich piano-stool shape complex) by DFT calculations. Fig. 8 shows optimized structures of $(C_6H_6)Cr(H_2)_n$ complexes from DFT calculations. Here, one Cr atom can bind up to three H_2 molecules (**4**, **5**, and **6** complexes in Fig. 8). In the $(C_6H_6)Cr(H_2)_3$ complex (**4**), one of the H_2 molecules (H3–H4) parallel to the benzene ring has a bond distance of 0.882 Å which is shorter than in the remaining two H_2 molecules (0.895 Å). The H_2 dissociation energies for **4**, **5**, and **6** complexes are 63.0, 65.9, and 76.3 kJ mol^{-1}, respectively, which are stronger than the ideal binding energy range (20–30 kJ mol^{-1}). Thus these complexes may suffer from desorption of H_2 at ambient conditions, however the higher binding energies indicate that it should be possible to achieve higher sorption capacities at room temperature, which is contrary to the experiment of Kaye and Long.[157] Lochan *et al.*[158] also considered other metals (V^-, Mn^+, Mo, and Mg^{2+}) instead of Cr and found that Mo and Mn^+ increase the H_2 binding energy by 84.4 kJ mol^{-1}, while Mg^{2+} leads to a decrease in the binding energy by 41.5 kJ mol^{-1}, and V^- shows a similar binding energy to the Cr case. In addition, similar to the MOF-5 with Cr metal centers,[157] Ti decorated MOF-5 was also proposed from DFT calculations.[159]

Incorporating coordinatively unsaturated metal centers within the organic linkers would be an alternative to enhance hydrogen storage capacity of MOFs at room temperature. However, the metal atoms bound to the organic linkers (*e.g.* benzene rings) in an η^6 fashion may have a lower binding energy to the organic linker than the cohesive energy of the metal crystal, leading to aggregation (clustering) of the metal,[160] which is also suggested by Kaye and Long.[157] If such clustering takes place, the Kubas interaction[139] between H_2 molecules and transition atoms becomes invalid. Owing to this clustering of the metal element, experimental H_2 uptake in MOF-5 with Cr metal centers on the benzene rings is very low at room temperature.[157] The clustering of transition metals in MOFs was also experimentally proven.[161,162]

This clustering of exposed metal atoms could be prevented by using another organic linker such as $[(Bipydc)M(CO)_4]^{2-}$ (Bipydc = 2,2′-bipyridine-5,5′-dicarboxylate) which is shown in Fig. 9(a). We calculated the binding energies of M^{n+} (M = Sc, Ti, V, Cr, Mn, Fe, Co, Ni, Cu and Zn, and n = 0, 1 and 2) to the Bipydc ligand by DFT calculations and then compared them with the cohesive energies of the transition metals. For n = 0, only Mn element has a stronger binding energy to the

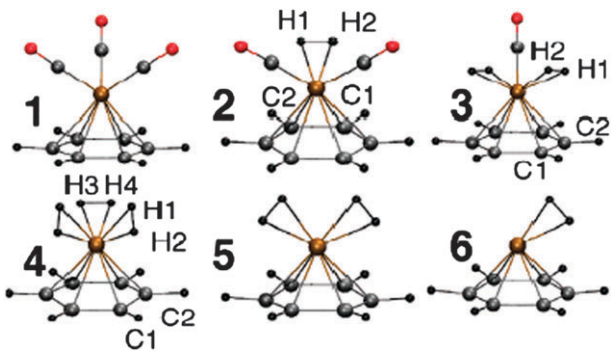

Fig. 8 Optimized structures of $(C_6H_6)Cr(CO)_{3-n}(H_2)_n$ (n = 0–3; **1–4**) and $(C_6H_6)Cr(H_2)_n$ (n = 1, 2; **5–6**) complexes from DFT calculations. Here the gray, red, black, and gold colors represent C, O, H, and Cr, respectively. Reproduced from ref. 158.

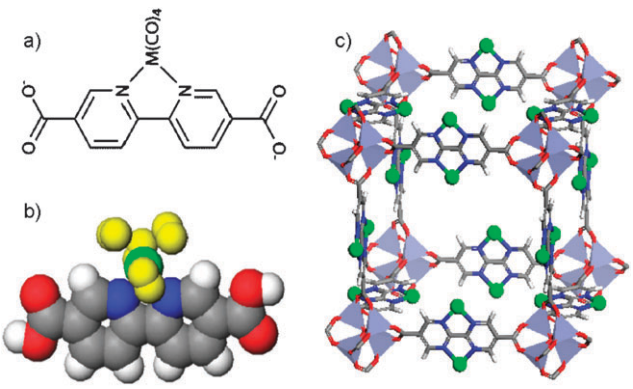

Fig. 9 (a) Molecular structure of the $[(Bipydc)M(CO)_4]^{2-}$ ligand, (b) the $(Bipydc)V^{2+}(H_2)_4$ structure optimized by DFT calculations where gray = C, white = H, red = O, blue = N, green = V, and yellow = H bonded to V, and (c) an atomistic structure of the MOF with the (Bipydc)V ligands.

Bipydc ligand than its cohesive energy. For $n = 1$, Mn^+, Co^+, Ni^+, Cu^+, and Zn^+ have stronger binding energies to the ligand. And in the case of $n = 2$, all metal elements are favorable for formation of the (Bipydc)M^{2+} complexes. Moreover, we investigated interactions between H_2 molecules and the (Bipydc)M^{2+} complexes and found that in (Bipydc)$M^{2+}(H_2)_4$ the average H_2 binding energies per H_2 molecule are from -24.6 kJ mol^{-1} for Zn^{2+} to -62.2 kJ mol^{-1} for V^{2+}, where the optimized structure of (Bipydc)$V^{2+}(H_2)_4$ is shown in Fig. 9(b). Since most of the binding energies are in the ideal values range for H_2 storage at room temperature, MOFs or COFs with the (Bipydc)M^{2+} complexes would be promising for practical hydrogen storage. We will report the detailed results in a future paper.

3.6 Doping of alkali elements onto the organic linker parts of MOFs (or COFs)

In 2007, we first proposed Li-doped MOFs as a practical hydrogen storage material using an *ab initio* based GCMC simulation shown in Fig. 10.[163] And predicted gravimetric H_2 adsorption isotherms for the Li-doped MOFs at 300 K are shown in Fig. 11. At 300 K, pure MOFs without Li doping lead to a low excess H_2 uptake of <1 wt% even at 100 bar although the total H_2 uptake is 2.5 wt% at 300 K and 100 bar, which is too low for practical use. However for Li-doped MOFs we predict significantly improved H_2 uptake at room temperature. For example, at 300 K and 20 bar we calculate that Li-MOF-C30 binds excess 3.89 wt% H_2 (total 4.21 wt% H_2), which goes up to 4.56 wt% H_2 (total 5.30 wt%). Besides, at a pressure of 100 bar, Li-MOF-C30 shows an excess H_2 uptake of 5.16 wt% (300 K), 5.57 wt% (273 K), and 5.99 wt% (243 K), and a total H_2 uptake of 6.47 wt% (300 K), 7.03 wt% (273 K), and 7.57 wt% (243 K), which reaches the

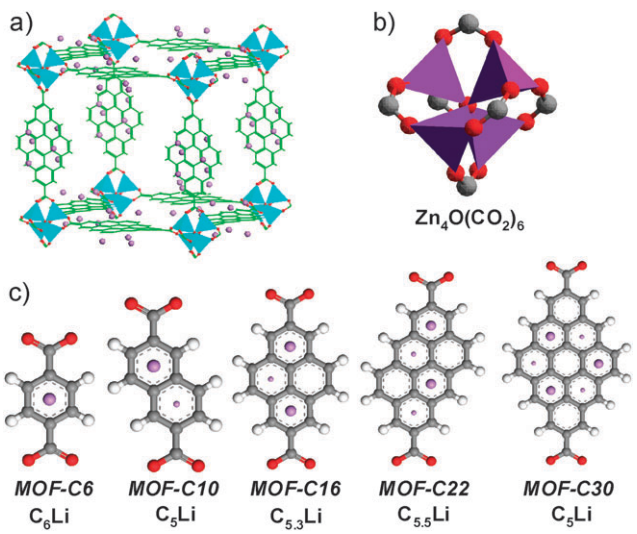

Fig. 10 Atomistic structures of Li-doped MOFs. An overview of the complete structure is shown in (a). Here, the purple tetrahedra correspond to the metallic nodes in (b), and the different linkers are shown in (c). In each case the $Zn_4O(CO_2)_6$ connector couples to six aromatic linkers through the O–C–O common to each linker. The large violet atoms in the linkers represent Li atoms above the linkers while the small violet Li atoms lie below the linkers. The C_xLi ratio considers only aromatic carbon atoms.

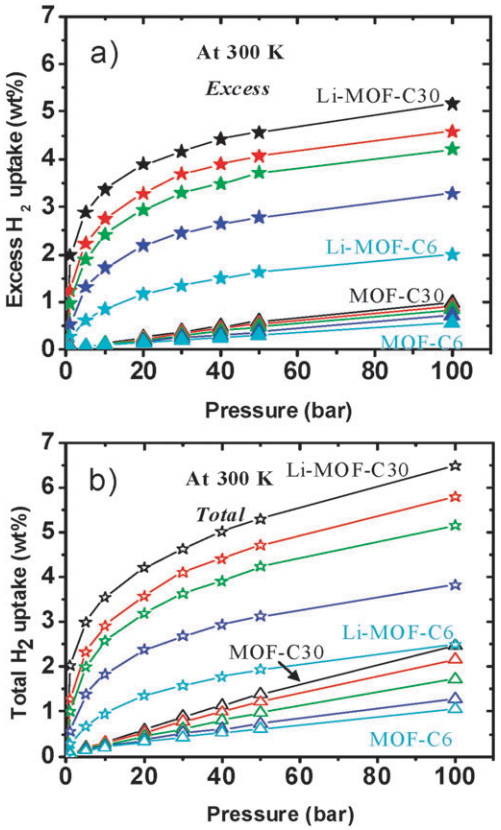

Fig. 11 Predicted excess (a) and total (b) H_2 adsorption isotherms in gravimetric units (wt%) at 300 K for pure MOFs (triangles) and Li-doped MOF (stars) systems. Note that Li-MOF-C30 achieves over excess 5 wt% and total 6.5 wt% at 100 bar. The color code is MOF-C6 = cyan, MOF-C10 = blue, MOF-C16 = green, MOF-C22 = red, and MOF-C30 = black.

2010 DOE target of 6.0 wt%. For Li-doped MOFs the high electron affinity of the aromatic sp^2 carbon framework promotes separation of the charge, making the Li positive (acidic), providing strong stabilization of molecular H_2 where the effective binding energy of H_2 is 16.8 kJ mol^{-1}.

After publishing the paper on Li-doped MOFs, some similar theoretical works were reported.[164–168] Blomqvist *et al.*[164] showed using DFT calculations that two Li atoms are strongly adsorbed on six-carbon rings of the organic linker in Zn_4-based MOF-5, one on each site, carrying a charge of $+0.9$ e per Li, and each Li can bind three H_2 molecules around itself with a binding energy of 12 kJ mol^{-1}. Mavrandonakis *et al.*[165] showed that the Li atom is preferably located on the organic linker in MOFs rather than the metal oxide part, and Li is positively charged by almost $+1$ e. Upon interacting with the H_2 molecules, strong polarization effects are observed and a charge distribution of approximately $+0.1$ e is transferred from the adsorbed three H_2 molecules to the Li atom, leading to very strong dipoles which is the reason for the strong binding.[165] However, another theoretical work[166] on Zn_2-based MOFs reported the result that the Li associates strongly with the metal oxide part and less so with the aromatic rings. Klontzas *et al.*[167] calculated the hydrogen storage amount in MOFs modified by lithium alkoxide groups, and the Li-modified MOFs have a high H_2 uptake

of 10 wt% at 77 K and 100 bar and 4.5 wt% at room temperature. Choi *et al.*[168] considered Li-doped COFs and showed using DFT calculations that Li doping plays a beneficial role to enhance H_2 uptake of COFs.

The Li doping effect on H_2 uptake in MOFs was also experimentally reported by Mulfort and Hupp.[169] They directly reduced a MOF of $Zn_2(ndc)_2(diPyNI)$ (ndc = 2,6-naphthalenedicarboxylate, diPyNI = *N*,*N*′-di-(4-pyridyl)-1,4,5,8-naphthalenetetracarboxydiimide) through a suspension of Li metal in DMF. This procedure allowed doping of Li^+ cations into the MOF, and the Li-doped MOF led to an increase in H_2 adsorption from 0.93 to 1.63 wt% at 77 K and 1 atm. They also experimentally investigated effects of Na^+ and K^+ doping on H_2 uptake in MOFs.[170] The experiment showed that H_2 binding is strongest with Li and decreases as $Li^+ > Na^+ > K^+$, however the uptake increases in the opposite order. The alkali-doped MOFs have the interwoven structure, which means that the alkali cations may be positioned between frameworks and thus not readily accessible to H_2. The heat of adsorption of H_2 in the alkali-doped MOFs is smaller than calculated in the theoretical results[163–165] mentioned above.

Next, we discuss the experimental synthesis of the Li-doped MOFs or COFs, especially aromatic lithium complexes in an η^6 coordination, from the literature since the Li-doped MOFs or COFs are most promising for practical hydrogen storage. Thus this examination of experimental evidence of the aromatic lithium complexes should provide important information for future experimental and theoretical studies.

The π-complexes between lithium and benzene derivatives bonded through η^6-coordination has been reported in many times in the literature. Stucky and co-workers[171] synthesized compound **7** (Fig. 12) which was synthesized under mild conditions from naphthalene and *n*-butyllithium (*n*-BuLi) in an ether–hexane solution. The procedure was undertaken at room temperature and in a glove box with an Ar atmosphere, which indicates the thermodynamic stability of the complex. However the compound is very sensitive to water and air.

In an analogous synthesis, Stucky and co-workers[172] reported derivative **8** (Fig. 13), which was synthesized from 9,10-dihydroanthracene and *n*-butyllithium. The solvent used was dry benzene and *N*,*N*,*N*′,*N*′-tetramethylethylenediamine under a nitrogen atmosphere. The lithium was added as *n*-butyllithium in hexane. Finally the solution was kept under a He atmosphere and no heat was necessary. They noticed that when the mixing was done, the solution turned to dark purple which suggested the formation of the anthracene dianion. The

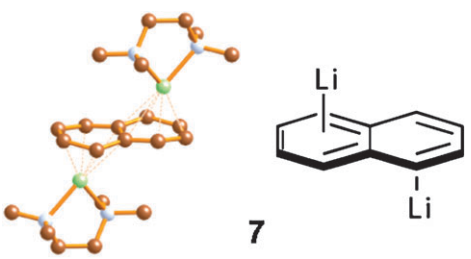

Fig. 12 Crystal structure (left) and idealized structure without solvent molecules (right) of compound **7**. Color code is Li = green, C = brown, and N = white. H is not shown for clarity.

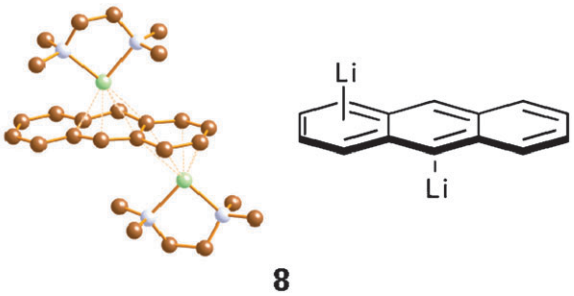

Fig. 13 Crystal structure (left) and idealized structure without solvent molecules (right) of compound **8**. Color code is Li = green, C = brown, and N = white. H is not shown for clarity.

crystal structure shows however that the benzene rings do not retain a planar orientation, as expected from the anthracenide fragment, which is antiaromatic. In a *tour de force* to form these complexes, Manceron and Andrews[173] used cryogenic conditions (~15 K) to mix benzene and lithium metal in solid argon. The authors reach the conclusion that LiC_6H_6 and $Li(C_6H_6)_2$ was formed using IR and isotopic studies.

The chemistry of η^6-benzene–Li complexes has proved to be feasible, however the η^5-Cp–Li system offers more versatility and stability. So if a porous material was to be targeted to form complexes with Li, Cp incorporation into the ligand would help to absorb the metal. Thus we propose some ligands with these characteristics in Fig. 14. Compounds analogous to **9** have been experimentally synthesized,[174] and some have been coordinated to transition metals.[175] Compound **10** is proposed to form a compound analogous to MOF-177. The source of Li for most of these systems comes from *n*-BuLi and the common solvents used are toluene, hexane, THF, and TMEDA. Common solvents used in the formation of microporous materials include these solvents, so there is an opportunity window to generate impregnation in solution with Li. Moreover the temperatures at which the reactions were executed include room temperature so the kinetic parameter should not be an obstacle. Lithium metal has been tried as the Li source but the reaction conditions are harsh so it is not a recommended path to obtain Li.

3.7 Substitution of the metal oxide parts in MOFs

Substitution of metal oxide units in MOFs with a lighter metal element could improve the hydrogen storage amount in

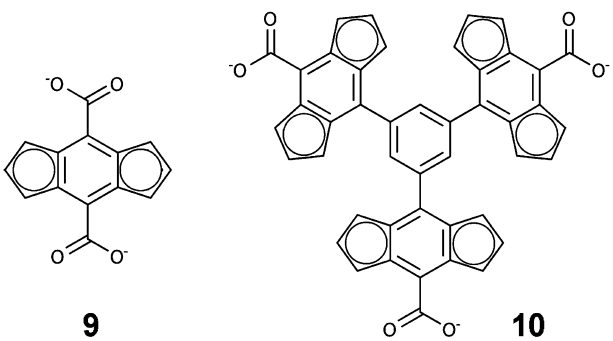

Fig. 14 Ligands proposed for the synthesis of new MOFs containing the group Cp.

gravimetric units owing to the lighter weight of the MOFs.[114] Férey *et al.*[176] synthesized $M(OH)(O_2C–C_6H_4–CO_2)$ ($M = Al^{3+}$, Cr^{3+}) called MIL-53 and found that Al^{3+} leads to a higher hydrogen storage amount of 3.8 wt% than Cr^{3+} (3.1 wt%) at 77 K and 1.6 MPa, showing that the lighter element is beneficial in gravimetric H_2 uptake. Dincã and Long[177] synthesized a MOF using Mg^{2+} ions and the MOF showed 0.46 wt% at 77 K and 880 torr. And Farha *et al.*[178] synthesized carborane (icosahedral carbon-containing boron clusters) based MOFs and the MOF stored 2.1 wt% H_2 at 77 K and 1 atm.

The substitution of metal oxides in MOFs can lead to an increase in the heat of adsorption of H_2. In Prussian blue analogues $M_3[Co(CN)_6]_2$ (M = Mn, Fe, Co, Ni, Cu, Zn),[179] the heat of adsorption of H_2 is changed with the metal and the order is Ni > Cu > Co > Fe > Zn > Mn, with the heat of adsorption in the range of 5.3 to 7.0 kJ mol^{-1}, much lower than the ideal value (20–30 kJ mol^{-1}) for practical hydrogen storage. Another similar work was also recently published.[180]

We also clarified the effects of the substitution of transition metals with lighter elements (Mg and Be) on H_2 uptake in the MOFs using *ab initio* and GCMC methodologies.[48] In the work, we used the MOF structures shown in Fig. 1. From MP2 calculations, we find that the $Mg_4O(CO_2)_6H_6$ cluster shows a slightly stronger H_2 binding energy (−6.78 kJ mol^{-1}) than that (−6.24 kJ mol^{-1}) of original $Zn_4O(CO_2)_6H_6$, while $Be_4O(CO_2)_6H_6$ has a lower H_2 binding energy (−4.40 kJ mol^{-1}). Simulated H_2 storage capacities of the Mg- and Be-MOFs are shown in Fig. 15. The substitution of Mg and Be increases H_2 uptake in the MOFs. For 77 K, excess H_2 uptake at 1 bar is 2.68 wt% for Mg-MOF, 1.38 wt% for Be-MOF, and 1.28 wt% for Zn-MOF, and the H_2 uptake at 100 bar is 7.63 wt% for Mg-MOF, 8.26 wt% for Be-MOF, and 5.09 wt% for Zn-MOF. Here, due to the strongest H_2 binding energy to the Mg cluster, the Mg-MOF has the highest H_2 uptake at low pressure (1 bar). It is noticeable that although the Be cluster has the weakest H_2 binding energy, the H_2 storage capacity is better than the Zn-MOF due to it having the lightest weight. However, at 300 K both the Mg- and Be-MOFs show much lower H_2 storage amounts than the 2010 DOE target (6.0 wt%) although they show higher H_2 storage than the Zn-MOF, indicating that this substitution of the metal oxide part with lighter elements may not guarantee the practical use of MOFs as a hydrogen storage material although this way would be helpful at cryogenic temperatures.

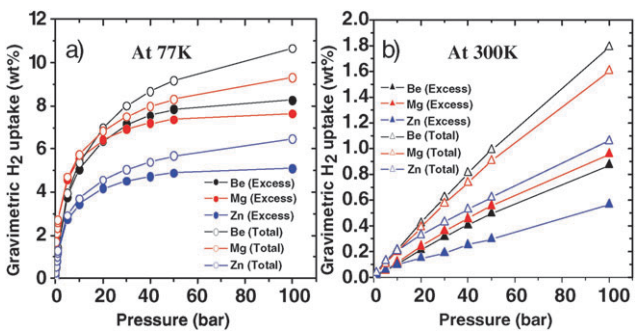

Fig. 15 Predicted H_2 adsorption isotherms for Zn-MOF-C6 (blue), Mg-MOF-C6 (red), and Be-MOF-C6 (black) at 77 (a) and 300 K (b). Here, solid and open symbols represent excess and total H_2 uptakes, respectively.

3.8 Functionalized organic linkers

As a way to increase the H_2 physisorption energy of MOFs, the functionalization of organic linkers would show a good effect. Currently, organic linkers of most MOFs have aromatic backbones such as benzene and naphthalene. According to the *ab initio* calculations performed so far, the H_2 physisorption energy to aromatic organic linkers increases with the addition of $–NH_2$, $–CH_3$, and –OH groups due to their ability to enrich the aromatic system electronically, however the energy increase is not significant.[30] The binding energy of H_2 to benzene is 3.91 kJ mol^{-1}, and it is 4.52 kJ mol^{-1} to $C_6H_5NH_2$, 4.40 kJ mol^{-1} to $C_6H_5CH_3$, and 4.00 kJ mol^{-1} to C_6H_5OH.[30] So the functionalized organic linkers could improve H_2 uptake at low temperature, but not significantly at ambient temperature. And the functionalized organic linkers may decrease the pore size of the MOF, leading to decrease in H_2 uptake at high pressure.

We theoretically investigated the effects of a single-linked aromatic ring and a polyaromatic ring (Fig. 16) on H_2 storage capacities of MOFs.[90] In pure MOF cases, the polyaromatic ring shows higher H_2 uptake at low pressure due to the higher H_2 heat of adsorption. Our MP2 calculations revealed that more aromatic rings lead to higher H_2 binding energies.[48] For example, H_2 binding energies to benzene and naphthalene are 3.81 and 4.27 kJ mol^{-1}, respectively.[48] However, a single-linked aromatic ring has generally a higher surface area and free volume than a polyaromatic linker because exposing the latent edges of the six-membered rings leads to a significant enhancement in specific surface area. Thus at high pressures a single-linked aromatic ring can store more H_2 than a poly-aromatic ring. However, both linkers still show low H_2 storage amounts (~1 wt%) at room temperature. On the other hand, in the Li-doped MOFs, a single-linked aromatic ring occupies the only C_6Li composition irrespective of the number of carbon atoms, while in a polyaromatic ring the greater number of carbon atoms can show a higher lithium concentration, leading to a significant increase in the heat of adsorption of H_2 due to the strong interaction between H_2 and Li.

3.9 Hydrogen spillover

The phenomenon of hydrogen spillover is defined as the dissociative chemisorption of hydrogen on the metal and the

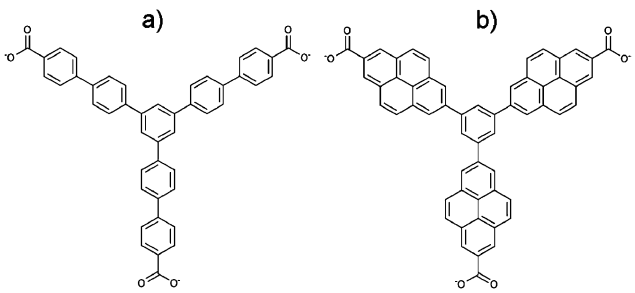

Fig. 16 Two different aromatic organic linkers: (a) a single-linked aromatic ring, and (b) a polyaromatic ring.

subsequent migration of atomic hydrogen onto the surface of the support such as alumina, carbon, and so on.[181]

For the first time, Li and Yang[182] applied this hydrogen spillover technique to MOF materials to enhance hydrogen storage at room temperature. They investigated the hydrogen spillover effect on hydrogen storage in IRMOF-1 and IRMOF-8 by using Pt on active carbon (Pt/AC) catalysts and then found that through this spillover of hydrogen atoms the hydrogen storage capacities of IRMOF-1 were significantly increased up to 1.6 wt% from 0.4 wt% for unmodified IRMOF-1 at 298 K and 10 MPa.[182] Similarly, the hydrogen storage amount of IRMOF-8 increased up to 1.8 wt% from 0.5 wt% at 298 K and 10 MPa through the hydrogen spillover technique.[182]

They also improved the spillover efficiency using carbon bridges at interfaces between the MOF and Pt/AC, and MOFs.[183] These carbon bridges led to a significant increase in the hydrogen storage capacity of the MOFs at room temperature. At 298 K and 10 MPa, IRMOF-1 stored 3 wt% H_2 and IRMOF-8 stored 4 wt% H_2. Moreover, this technique was also applied to MOF-177.[184] Here it is also noticeable that the hydrogen storage capacity by the hydrogen spillover is reversible.

Although hydrogen storage by spillover must be a promising technique to achieve significant hydrogen storage in MOFs, the topic has been not actively studied theoretically. The only theoretical work was reported by Li *et al.*[185] where they calculated adsorption energies of a hydrogen atom in MOFs with DFT calculations.

Our research group recently developed a new simulational paradigm called a reactive force field (ReaxFF).[186] With this ReaxFF, one can accurately simulate chemical reactions (bond formation and breaking) in large systems. Thus, we expect that this simulation technique will be very helpful to study the hydrogen spillover phenomenon in MOFs.

4. Conclusions

This critical review summarizes the state of the art for theoretical studies of hydrogen storage in MOFs and COFs, showing that *in silico* methodology can provide important information (*e.g.* hydrogen adsorption site, hydrogen storage capacity, and hydrogen diffusion) to guide development of improved hydrogen storage materials. The H_2 adsorption sites in MOFs and COFs are based on quantum mechanical calculations, either *ab initio* (*e.g.* MP2) or DFT. Hydrogen storage capacity in these porous materials can be predicted using GCMC simulations. Here, the accuracy of the GCMC simulation depends on the accuracy of the FFs describing the interatomic interactions for host–guest and guest–guest. Many, theoretical studies have used empirical FFs for the GCMC simulation, which have led to discrepancies between simulation and experiment. This problem can be solved by using FFs developed from accurate *ab initio* calculations. Here, we summarize our previous results showing that *ab initio* based GCMC simulations reproduce well experimental excess H_2 adsorption isotherms for MOFs and COFs leading to accurate total H_2 predictions. Moreover, kinetic properties of H_2 in MOFs and COFs can be predicted by MD simulations.

Based on theoretical and experimental studies on H_2 uptake in MOFs and COFs, we discussed nine strategies to improve the hydrogen storage capacity of MOFs and COFs. Among these strategies, only three (open transition metal sites within the organic linker using the Kubas interaction, doping of alkali elements on the organic linker, and hydrogen spillover) lead to high hydrogen storage at room temperature. For example, with Li-doped MOFs we predict H_2 storage of more than 6 wt% near room temperature, meeting the 2010 DOE target. However, the other six strategies would be helpful at cryogenic temperatures. We hope that this review will provide useful guidelines for improved designs of MOFs or COFs as a hydrogen storage material.

Acknowledgements

We thank Prof. Omar Yaghi for introducing us to the world of MOFs, COFs, and ZIFs with their fascinating chemistries and applications. We thank the DOE for funding (initiated with DE-FG01-04ER04-20 and completed with DE-PS36-08GO98004P).

References

1 L. Schlapbach and A. Züttel, *Nature*, 2001, **414**, 353.
2 J. M. Ogden, *Annu. Rev. Energy Environ.*, 1999, **24**, 227.
3 A. M. Seayad and D. M. Antonelli, *Adv. Mater.*, 2004, **16**, 765.
4 R. E. Morris and P. S. Wheatley, *Angew. Chem., Int. Ed.*, 2008, **47**, 4966.
5 U.S. Department of Energy. Energy Efficiency and Renewable Energy. http://www.eere.energy.gov/hydrogenandfuelcells/pdfs/freedomcar_targets_explanations.pdf. Also available from the authors.
6 H. W. Langmi and G. S. McGrady, *Coord. Chem. Rev.*, 2007, **251**, 925.
7 W. J. Nellis, A. A. Louis and N. W. Ashcroft, *Philos. Trans. R. Soc. London, Ser. A*, 1998, **356**, 119; Y. Li and R. T. Yang, *J. Phys. Chem. B*, 2006, **110**, 17175.
8 A. C. Dillon, K. M. Jones, T. A. Bekkedahl, C. H. Kiang, D. S. Bethune and M. J. Heben, *Nature*, 1997, **386**, 377; M. Hirscher, *Appl. Phys. A*, 2001, **72**, 2; B. Panella, M. Hirscher and S. Roth, *Carbon*, 2005, **43**, 2209; P. Benard and R. Chanhine, *Scr. Mater.*, 2007, **56**, 803.
9 R. Ma, Y. Bando, H. Zhu, T. Sato, C. Xu and D. Wu, *J. Am. Chem. Soc.*, 2002, **124**, 7672; S. S. Han, J. K. Kang, H. M. Lee, A. C. T. van Duin and W. A. Goddard III, *J. Chem. Phys.*, 2005, **123**, 114704; S. S. Han, S. H. Lee, J. K. Kang and H. M. Lee, *Phys. Rev. B*, 2005, **72**, 113402.
10 P. K. Thallapally, G. O. Lloyd, T. B. Wirsig, M. W. Bredenkamp, J. L. Atwood and L. J. Barbour, *Chem. Commun.*, 2005, 5272; N. B. McKeown, B. Gahnem, K. J. Msayib, P. M. Budd, C. E. Tattershall, K. Mahmood, S. Tan, D. Book, H. W. Langmi and A. Walton, *Angew. Chem., Int. Ed.*, 2006, **45**, 1804; P. M. Budd, A. Butler, J. Selbie, K. Mahmood, N. B. McKeown, B. Ghanem, K. Msayib, D. Book and A. Walton, *Phys. Chem. Chem. Phys.*, 2007, **9**, 1802.
11 H. Li, M. Eddaoudi, M. O'Keeffe and O. M. Yaghi, *Nature*, 1999, **402**, 276.
12 O. M. Yaghi, M. O'Keeffe, N. W. Ockwig, H. K. Chae, M. Eddaoudi and J. Kim, *Nature*, 2003, **423**, 705.
13 N. L. Rosi, J. Eckert, M. Eddaoudi, D. T. Vodak, J. Kim, M. O'Keeffe and O. M. Yaghi, *Science*, 2003, **300**, 1127.
14 J. L. C. Rowsell, A. R. Millward, K. S. Park and O. M. Yaghi, *J. Am. Chem. Soc.*, 2004, **126**, 5666.
15 S. S. Kaye, A. Daily, O. M. Yaghi and J. R. Long, *J. Am. Chem. Soc.*, 2007, **129**, 14176.
16 A. G. Wong-Foy, A. J. Matzger and O. M. Yaghi, *J. Am. Chem. Soc.*, 2006, **128**, 3494.

17 M. Dincă, A. Dailly, Y. Liu, C. M. Brown, D. A. Neumann and J. R. Long, *J. Am. Chem. Soc.*, 2006, **128**, 16876.
18 A. P. Côté, A. I. Benin, N. W. Ockwig, M. O'Keeffe, A. J. Matzger and O. M. Yaghi, *Science*, 2005, **310**, 1166.
19 A. P. Côté, H. M. El-Kaderi, H. Furukawa, J. R. Hunt and O. M. Yaghi, *J. Am. Chem. Soc.*, 2007, **129**, 12914.
20 H. M. El-Kaderi, J. R. Hunt, J. L. Mendoza-Cortés, A. P. Côté, R. E. Taylor, M. O'Keeffe and O. M. Yaghi, *Science*, 2007, **316**, 268.
21 J. R. Hunt, C. J. Doonan, J. D. LeVangie, A. P. Côté and O. M. Yaghi, *J. Am. Chem. Soc.*, 2008, **130**, 11872.
22 A. L. Myers, J. A. Calles and G. Calleja, *Adsorption*, 1997, **3**, 107.
23 S. Sircar, *Ind. Eng. Chem. Res.*, 1999, **38**, 3670.
24 H. Furukawa, M. A. Miller and O. M. Yaghi, *J. Mater. Chem.*, 2007, **17**, 3197.
25 A. V. Neimark and P. I. Ravikovitch, *Langmuir*, 1997, **13**, 5148.
26 National Institute of Standards and Technology. http://webbook.nist.gov/chemistry/fluid/.
27 M. Eddaoudi, J. Kim, N. Rosi, D. Vodak, J. Wachter, M. O'Keeffe and O. M. Yaghi, *Science*, 2002, **295**, 469.
28 C.-I. Weng, S.-P. Ju, K.-C. Fang and F.-P. Chang, *Comput. Mater. Sci.*, 2007, **40**, 300.
29 S. P. Chan, M. Ji, X. G. Gong and Z. F. Liu, *Phys. Rev. B*, 2004, **69**, 092101.
30 O. Hüber, A. Glöss, M. Fichtner and W. Klopper, *J. Phys. Chem. A*, 2004, **108**, 3019.
31 C. Møller and M. S. Plesset, *Phys. Rev.*, 1934, **46**, 618.
32 R. Ahlrichs, M. Bär, M. Häser, H. Horn and C. Kölmel, *Chem. Phys. Lett.*, 1989, **162**, 165; F. Weigend and M. Häser, *Theor. Chem. Acc.*, 1997, **97**, 331; F. Weigend, M. Häser, H. Patzelt and R. Ahlrichs, *Chem. Phys. Lett.*, 1998, **294**, 143.
33 A. Schäfer, C. Huber and R. Ahlrichs, *J. Chem. Phys.*, 1994, **100**, 5829.
34 T. H. Dunning, *J. Chem. Phys.*, 1989, **90**, 1007.
35 T. Sagara, J. Klassen and E. Ganz, *J. Chem. Phys.*, 2004, **121**, 12543.
36 S. Hamel and M. Côté, *J. Chem. Phys.*, 2004, **121**, 12618.
37 J. A. Pople, M. Head-Gordon and K. Raghavachari, *J. Chem. Phys.*, 1987, **87**, 5968.
38 S. H. Vosko, L. Wilk and M. Nusair, *Can. J. Phys.*, 1980, **58**, 1200.
39 J. P. Perdew, K. Burke and M. Ernzerhof, *Phys. Rev. Lett.*, 1996, **77**, 3865; J. P. Perdew, K. Burke and M. Ernzerhof, *Phys. Rev. Lett.*, 1997, **78**, 1396.
40 T. Sagara, J. Kassen and E. Ganz, *J. Chem. Phys.*, 2005, **123**, 014701.
41 T. Sagara, J. Orthony and E. Ganz, *J. Chem. Phys.*, 2005, **123**, 214707.
42 C. Buda and B. D. Dunietz, *J. Phys. Chem. B*, 2006, **110**, 10479.
43 R. C. Lochan and M. Head-Gordon, *Phys. Chem. Chem. Phys.*, 2006, **8**, 1357.
44 F. Negri and N. Saending, *Theor. Chem. Acc.*, 2007, **118**, 149.
45 E. Klontzas, A. Mavrandonakis, G. E. Froudakis, Y. Carissan and W. Klopper, *J. Phys. Chem. C*, 2007, **111**, 13635.
46 Y. Gao and X. C. Zeng, *J. Phys.: Condens. Matter*, 2007, **19**, 386220.
47 T. B. Lee, D. Kim, D. H. Jung, S. B. Choi, J. H. Yoon, J. Kim, K. Choi and S.-H. Choi, *Catal. Today*, 2007, **120**, 330.
48 S. S. Han, W.-Q. Deng and W. A. Goddard III, *Angew. Chem., Int. Ed.*, 2007, **46**, 6289.
49 T. Sagara and E. Ganz, *J. Phys. Chem. C*, 2008, **112**, 3515.
50 A. Kuc, T. Heine, G. Seifert and H. A. Duarte, *Chem.–Eur. J.*, 2008, **14**, 6597.
51 F. M. Mulder, T. J. Dingemans, M. Wagemaker and G. J. Kearley, *Chem. Phys.*, 2005, **317**, 113.
52 T. Mueller and G. Ceder, *J. Phys. Chem. B*, 2005, **109**, 17974.
53 J. L. C. Rowsell, E. C. Spencer, J. Eckert, J. A. K. Howard and O. M. Yaghi, *Science*, 2005, **309**, 1350.
54 J. L. C. Rowsell, J. Eckert and O. M. Yaghi, *J. Am. Chem. Soc.*, 2005, **127**, 14904.
55 T. Yildirim and M. R. Hartman, *Phys. Rev. Lett.*, 2005, **95**, 215504.
56 S. Bordiga, J. G. Vitillo, G. Ricchiardi, L. Regli, D. Cocina, A. Zecchina, B. Arstad, M. Bjørgen, J. Hafizovic and K. P. Lillerud, *J. Phys. Chem. B*, 2005, **109**, 18237.
57 E. C. Spencer, J. A. K. Howard, G. J. McIntyre, J. L. C. Rowsell and O. M. Yaghi, *Chem. Commun.*, 2006, 278.
58 L. Zhang, Q. Wang and Y.-C. Liu, *J. Phys. Chem. B*, 2007, **111**, 4291.
59 S. Kristyan and P. Pulay, *Chem. Phys. Lett.*, 1994, **229**, 175.
60 T. van Mourik and R. J. Gdanitz, *J. Chem. Phys.*, 2002, **116**, 9620.
61 S. K. Bhatia and A. L. Myers, *Langmuir*, 2006, **22**, 1688.
62 N. Metropolis, A. W. Rosenbluth, M. N. Rosenbluth, A. N. Teller and E. Teller, *J. Chem. Phys.*, 1953, **21**, 1087.
63 A. Rappé, C. J. Casewit, K. S. Colwell, W. A. Goddard III and W. M. Skiff, *J. Am. Chem. Soc.*, 1992, **114**, 10024.
64 Q. Yang and C. Zhong, *J. Phys. Chem. B*, 2005, **109**, 11862.
65 W. L. Jorgensen, D. S. Maxwell and J. Tirado-Rives, *J. Am. Chem. Soc.*, 1996, **118**, 11225.
66 G. Garberoglio, A. I. Skoulidas and J. K. Johnson, *J. Phys. Chem. B*, 2005, **109**, 13094.
67 H. Li, M. Eddaoudi, T. L. Groy and O. M. Yaghi, *J. Am. Chem. Soc.*, 1998, **120**, 8571.
68 M. Eddaoudi, H. Li and O. M. Yaghi, *J. Am. Chem. Soc.*, 2000, **122**, 1391.
69 S. Mayo, B. Olafson and W. A. Goddard III, *J. Phys. Chem.*, 1990, **94**, 8897.
70 R. P. Feynman, *Rev. Mod. Phys.*, 1948, **20**, 367.
71 Q. Yang and C. Zhong, *J. Phys. Chem. B*, 2006, **110**, 17776.
72 S. S.-Y. Chui, S. M.-F. Lo, J. P. H. Charmant, A. G. Orpen and I. D. Williams, *Science*, 1999, **283**, 1148.
73 B. Panella, M. Hirsher, H. Pütter and U. Müller, *Adv. Funct. Mater.*, 2006, **16**, 520.
74 B. L. Chen, N. W. Ockwig, A. R. Millward, D. S. Contreras and O. M. Yaghi, *Angew. Chem., Int. Ed.*, 2005, **44**, 4745.
75 Q. Yang and C. Zhong, *J. Phys. Chem. B*, 2006, **110**, 655.
76 H. Frost, T. Düren and R. Q. Snurr, *J. Phys. Chem. B*, 2006, **110**, 9565.
77 D. H. Jung, D. Kim, T. B. Lee, S. B. Choi, J. H. Yoon, J. Kim, K. Choi and S.-H. Choi, *J. Phys. Chem. B*, 2006, **110**, 22987.
78 P. Ryan, L. J. Broadbelt and R. Q. Snurr, *Chem. Commun.*, 2008, 4132.
79 J. Liu, J. Y. Lee, L. Pan, R. T. Obermyer, S. Simizu, B. Zande, J. Li, S. G. Sankar and J. K. Johnson, *J. Phys. Chem. C*, 2008, **112**, 2911.
80 J. Liu, J. T. Culp, S. Natesakhawat, B. C. Bockrath, B. Zande, S. G. Sankar, G. Garberoglio and J. K. Johnson, *J. Phys. Chem. C*, 2007, **111**, 9305.
81 D. Noguchi, H. Tanaka, A. Kondo, H. Kajiro, H. Noguchi, T. Ohba, H. Kanoh and K. Kaneko, *J. Am. Chem. Soc.*, 2008, **130**, 6367.
82 L. Zhang, Q. Wang and Y.-C. Liu, *J. Phys. Chem. B*, 2007, **111**, 4291.
83 H. Frost and R. Q. Snurr, *J. Phys. Chem. C*, 2007, **111**, 18794.
84 G. Garberoglio, *Langmuir*, 2007, **23**, 12154.
85 E. Klontzas, E. Tylianakis and G. E. Froudakis, *J. Phys. Chem. C*, 2008, **112**, 9095.
86 A. Michels, W. Degraaff and C. A. Tenseldam, *Physica*, 1960, **26**, 393.
87 G. Garberoglio and R. Vallauri, *Microporous Mesoporous Mater.*, 2008, **116**, 540.
88 V. Buch, *J. Chem. Phys.*, 1994, **100**, 7610.
89 F. Darkrim and D. Levesque, *J. Chem. Phys.*, 1998, **109**, 4981.
90 S. S. Han and W. A. Goddard III, *J. Phys. Chem. C*, 2008, **112**, 13431.
91 S. S. Han, H. Furukawa, O. M. Yaghi and W. A. Goddard III, *J. Am. Chem. Soc.*, 2008, **130**, 11580.
92 W. Q. Deng, X. Xu and W. A. Goddard III, *Phys. Rev. Lett.*, 2004, **92**, 166103.
93 H. K. Chae, D. Y. Siberio-Perez, J. Kim, Y.-B. Go, M. Eddaoudi, A. J. Matzger, M. O'Keeffe and O. M. Yaghi, *Nature*, 2004, **427**, 523.
94 J. L. Mendoza-Cortés, S. S. Han, H. Furukawa, O. M. Yaghi and W. A. Goddard III, unpublished work.
95 W. Zhou, H. Wu, M. R. Hartman and T. Yildirim, *J. Phys. Chem. C*, 2007, **111**, 16131.
96 A. I. Skoulidas and D. S. Sholl, *J. Phys. Chem. B*, 2005, **109**, 15760.
97 D. Dubbeldam and R. Q. Snurr, *Mol. Simul.*, 2007, **33**, 305.

98 B. Liu, Q. Yang, C. Xue, C. Zhong and B. Smit, *Phys. Chem. Chem. Phys.*, 2008, **10**, 3244.
99 S. Keskin, J. Liu, J. K. Johnson and D. S. Sholl, *Langmuir*, 2008, **24**, 8254.
100 F. Salles, H. Jobic, G. Maurin, M. M. Koza, P. L. Llewellyn, T. Devic, C. Serre and G. Ferey, *Phys. Rev. Lett.*, 2008, **100**, 245901.
101 K. Barthelet, J. Marrot, D. Riou and G. Férey, *Angew. Chem., Int. Ed.*, 2002, **41**, 281.
102 C. Serre, F. Millange, C. Thouvenot, M. Noguès, G. Marsolier, D. Louër and G. Férey, *J. Am. Chem. Soc.*, 2002, **124**, 13519.
103 N. Rosenbach, H. Jobic, A. Ghoufi, F. Salles, G. Maurin, S. Bourrelly, P. L. Llewellyn, T. Devic, C. Serre and G. Férey, *Angew. Chem., Int. Ed.*, 2008, **47**, 6611.
104 S. S. Han and W. A. Goddard III, *J. Phys. Chem. C*, 2007, **111**, 15185.
105 D. Dubbeldam, K. S. Walton, D. E. Ellis and R. Q. Snurr, *Angew. Chem., Int. Ed.*, 2007, **46**, 4496.
106 W. Zhou, H. Wu, T. Yildirim, J. R. Simpson and A. R. Hight Walker, *Phys. Rev. B*, 2008, **78**, 054114.
107 M. Tafipolsky, S. Amirjalayer and R. Schmid, *J. Comput. Chem.*, 2007, **28**, 1169.
108 B. L. Huang, A. J. H. McGaughey and M. Kaviany, *Int. J. Heat Mass Transfer*, 2007, **50**, 393.
109 J. A. Greathouse and M. D. Allendorf, *J. Phys. Chem. C*, 2008, **112**, 5795.
110 R. Schmid and M. Tafipolsky, *J. Am. Chem. Soc.*, 2008, **130**, 12600.
111 N. L. Allinger, Y. H. Yuh and J.-H. Lii, *J. Am. Chem. Soc.*, 1989, **111**, 8551.
112 S. Amirjalayer, M. Tafipolsky and R. Schmid, *Angew. Chem., Int. Ed.*, 2007, **46**, 463.
113 P. Dauber-Osguthorpe, V. A. Roberts, D. J. Osguthorpe, J. Wolff, M. Genest and A. T. Hagler, *Proteins: Struct., Funct., Genet.*, 1988, **4**, 31.
114 J. L. C. Rowsell and O. M. Yaghi, *Angew. Chem., Int. Ed.*, 2005, **44**, 4670.
115 B. Panella and M. Hirscher, *Adv. Mater.*, 2005, **17**, 538.
116 A. Dailly, J. J. Vajo and C. C. Ahn, *J. Phys. Chem. B*, 2006, **110**, 1099.
117 X. Lin, J. Jia, X. Zhao, K. M. Thomas, A. J. Blake, G. S. Walker, N. R. Champness, P. Hubberstey and M. Schröder, *Angew. Chem., Int. Ed.*, 2006, **45**, 7358.
118 M. Latroche, S. Surblé, C. Serre, C. Mellot-Draznieks, P. L. Llewellyn, J.-H. Lee, J.-S. Chang, S. H. Jhung and G. Férey, *Angew. Chem., Int. Ed.*, 2006, **45**, 8227.
119 K. S. Walton and R. Q. Snurr, *J. Am. Chem. Soc.*, 2007, **129**, 8552.
120 S. M. Humphrey, J.-S. Chang, S. H. Jhung, J. W. Yoon and P. T. Wood, *Angew. Chem., Int. Ed.*, 2007, **46**, 272.
121 B. Panella, K. Hönes, U. Müller, N. Thukhan, M. Schubert, H. Pütter and M. Hirscher, *Angew. Chem., Int. Ed.*, 2008, **47**, 2138.
122 J. T. Culp, S. Natesakhawat, M. R. Smith, E. Bittner, C. Matranga and B. Bockrath, *J. Phys. Chem. C*, 2008, **112**, 7079.
123 R. W. Tilford, S. J. Mugavero III, P. J. Pellechia and J. J. Lavigne, *Adv. Mater.*, 2008, **20**, 2741.
124 S. S. Han, H. S. Kim, K. S. Han, J. Y. Lee, H. M. Lee, J. K. Kang, S. I. Woo, A. C. T. van Duin and W. A. Goddard III, *Appl. Phys. Lett.*, 2005, **87**, 213113.
125 S. Patchkovskii, J. S. Tse, S. N. Yurchenko, L. Zhechkov, T. Heine and G. Seifert, *Proc. Natl. Acad. Sci. U. S. A.*, 2005, **102**, 10439.
126 I. Cabria, M. J. López and J. A. Alonso, *Carbon*, 2007, **45**, 2649.
127 R. S. Aga, C. L. Fu, M. Krčmar and J. R. Morris, *Phys. Rev. B*, 2007, **76**, 165404.
128 S. S. Han and H. M. Lee, *Carbon*, 2004, **42**, 2169.
129 O. M. Yaghi, *Nat. Mater.*, 2007, **6**, 92.
130 T. K. Maji, R. Matsuda and S. Kitagawa, *Nat. Mater.*, 2007, **6**, 142.
131 B. Chen, M. Eddaoudi, S. T. Hyde, M. O'Keeffe and O. M. Yaghi, *Science*, 2001, **291**, 1021.
132 B. Kesanli, Y. Cui, M. R. Smith, E. W. Bittner, B. C. Bockrath and W. Lin, *Angew. Chem., Int. Ed.*, 2005, **44**, 72.
133 D. Sun, S. Ma, Y. Ke, D. J. Collins and H.-C. Zhou, *J. Am. Chem. Soc.*, 2006, **128**, 3896.
134 J. L. C. Rowsell and O. M. Yaghi, *J. Am. Chem. Soc.*, 2006, **128**, 1304.
135 B. Chen, S. Ma, F. Zapata, E. B. Lobkovsky and J. Yang, *Inorg. Chem.*, 2006, **45**, 5718.
136 S. Ma, D. Sun, M. Ambrogio, J. A. Fillinger, S. Parkin and H.-C. Zhou, *J. Am. Chem. Soc.*, 2007, **129**, 1858.
137 M. Xue, S. Ma, Z. Jin, R. M. Schaffino, G.-S. Zhu, E. B. Lobkovsky, S.-L. Qiu and B. Chen, *Inorg. Chem.*, 2008, **47**, 6825.
138 T. Gadzikwa, B.-S. Zeng, J. T. Hupp and S. T. Nguyen, *Chem. Commun.*, 2008, 3672.
139 G. J. Kubas, *Chem. Rev.*, 2007, **107**, 4152.
140 P. M. Forster, J. Eckert, J.-S. Chang, S.-E. Park, G. Férey and A. K. Cheetham, *J. Am. Chem. Soc.*, 2003, **125**, 1309.
141 M. Dincã, A. F. Yu and J. R. Long, *J. Am. Chem. Soc.*, 2006, **128**, 8904.
142 S. Ma and H.-C. Zhou, *J. Am. Chem. Soc.*, 2006, **128**, 11734.
143 P. M. Forster, J. Eckert, B. D. Heiken, J. B. Parise, J. W. Yoon, S. H. Jhung, J.-S. Chang and A. K. Cheetham, *J. Am. Chem. Soc.*, 2006, **128**, 16846.
144 X. Lin, J. Jia, P. Hubberstey, M. Schröder and N. R. Champness, *CrystEngComm*, 2007, **9**, 438.
145 D. J. Collins and H.-C. Zhou, *J. Mater. Chem.*, 2007, **17**, 3154.
146 M. Dincã and J. R. Long, *J. Am. Chem. Soc.*, 2007, **129**, 11172.
147 M. Dincã, W. S. Han, Y. Liu, A. Dailly, C. M. Brown and J. R. Long, *Angew. Chem., Int. Ed.*, 2007, **46**, 1419.
148 X.-S. Wang, S. Ma, P. M. Forster, D. Yuan, J. Eckert, J. J. López, B. J. Murphy, J. B. Parise and H.-C. Zhou, *Angew. Chem., Int. Ed.*, 2008, **47**, 7263.
149 B. Chen, X. Zhao, A. Putkham, K. Hong, E. B. Lobkovsky, E. J. Hurtado, A. J. Fletcher and K. M. Thomas, *J. Am. Chem. Soc.*, 2008, **130**, 6411.
150 J. G. Vitillo, L. Regli, S. Chavan, G. Ricchiardi, G. Spoto, P. D. C. Dietzel, S. Bordiga and A. Zecchina, *J. Am. Chem. Soc.*, 2008, **130**, 8386.
151 H. Chun, H. Jung, G. Koo, H. Jeong and D.-K. Kim, *Inorg. Chem.*, 2008, **47**, 5355.
152 W. Zhou, H. Wu and T. Yildirim, *J. Am. Chem. Soc.*, 2008, **130**, 15268.
153 M. Dincã and J. R. Long, *Angew. Chem., Int. Ed.*, 2008, **47**, 6766.
154 N. L. Rosi, J. Kim, M. Eddaoudi, B. L. Chen, M. O'Keeffe and O. M. Yaghi, *J. Am. Chem. Soc.*, 2005, **127**, 1504.
155 M. Kosa, M. Krack, A. K. Cheetham and M. Parrinello, *J. Phys. Chem. C*, 2008, **112**, 16171.
156 Y. Y. Sun, Y.-H. Kim and S. B. Zhang, *J. Am. Chem. Soc.*, 2007, **129**, 12606.
157 S. S. Kaye and J. R. Long, *J. Am. Chem. Soc.*, 2008, **130**, 806.
158 R. C. Lochan, R. Z. Khaliullin and M. Head-Gordon, *Inorg. Chem.*, 2008, **47**, 4032.
159 D. H. Jung, D. Kim, S.-H. Choi, J. Kim and K. Choi, *J. Korean Phys. Soc.*, 2008, **52**, 1221.
160 Q. Sun, Q. Wang, P. Jena and Y. Kawazoe, *J. Am. Chem. Soc.*, 2005, **127**, 14582.
161 S. Hermes, M.-K. Schroeter, R. Schmid, L. Khodeir, M. Muhler, A. Tissler, R. W. Fischer and R. A. Fischer, *Angew. Chem., Int. Ed.*, 2005, **44**, 6237.
162 F. Schröder, D. Esken, M. Cokoja, M. W. E. van den Berg, O. I. Lebedev, G. V. Tendeloo, B. Walaszek, G. Buntkowsky, H.-H. Limbach, B. Chaudret and R. A. Fischer, *J. Am. Chem. Soc.*, 2008, **130**, 6119.
163 S. S. Han and W. A. Goddard III, *J. Am. Chem. Soc.*, 2007, **129**, 8422.
164 A. Blomqvist, C. M. Araújo, P. Srepusharawoot and R. Ahuja, *Proc. Natl. Acad. Sci. U. S. A.*, 2007, **104**, 20173.
165 A. Mavrandonakis, E. Tylianakis, A. K. Stubos and G. E. Froudakis, *J. Phys. Chem. C*, 2008, **112**, 7290.
166 P. Dalach, H. Frost, R. Q. Snurr and D. E. Ellis, *J. Phys. Chem. C*, 2008, **112**, 9278.
167 E. Klontzas, A. Mavrandonakis, E. Tylianakis and G. E. Froudakis, *Nano Lett.*, 2008, **8**, 1572.
168 Y. J. Choi, J. W. Lee, J. H. Choi and J. K. Kang, *Appl. Phys. Lett.*, 2008, **92**, 173102.
169 K. L. Mulfort and J. T. Hupp, *J. Am. Chem. Soc.*, 2007, **129**, 9604.
170 K. L. Mulfort and J. T. Hupp, *Inorg. Chem.*, 2008, **47**, 7936.

171 J. J. Brooks, W. E. Rhine and G. D. Stucky, *J. Am. Chem. Soc*., 1972, **94**, 7346.
172 W. E. Rhine, J. Davis and G. D. Stucky, *J. Am. Chem. Soc*., 1975, **97**, 2079.
173 L. Manceron and L. Andrews, *J. Am. Chem. Soc*., 1988, **110**, 3840.
174 K. Hafner, B. Stowasser, H.-P. Krimmer, S. Fischer, M. C. Bohm and H. J. Lindner, *Angew. Chem., Int. Ed. Engl*., 1986, **25**, 630; J. D. Dunitz, C. Kruger, H. Irngartinger, E. F. Maverick, Y. Wang and M. Nixdorf, *Angew. Chem., Int. Ed. Engl*., 1988, **27**, 387; T. Kubo, A. Shimizu, M. Sakamoto, M. Uruichi, K. Yakushi, M. Nakano, D. Shiomi, K. Sato, T. Takui, Y. Morita and K. Nakasuji, *Angew. Chem., Int. Ed*., 2005, **44**, 6564.
175 W. L. Bell, C. J. Curtis, C. W. Eigenbrot, C. G. Pierpont, J. L. Robbins and J. C. Smart, *Organometallics*, 1987, **6**, 266; D. R. Cary, C. G. Webster, M. J. Drewitt, S. Barlow, J. C. Green and D. O'Hare, *Chem. Commun*., 1997, 953; P. Roussel, D. R. Cary, S. Barlow, J. C. Green, F. Varret and D. O'Hare, *Organometallics*, 2000, **19**, 1071; E. Esponda, C. Adams, F. Burgos, I. Chavez, J. M. Manriquez, F. Delpech, A. Castel, H. Gornitzka, M. Riviere-Baudet and P. Riviere, *J. Organomet. Chem*., 2006, **691**, 3011; J. M. Manriquez, M. D. Ward, W. M. Reiff, J. C. Calabrese, N. L. Jones, P. J. Carroll, E. E. Bunel and J. S. Miller, *J. Am. Chem. Soc*., 1995, **117**, 6182.
176 G. Férey, M. Latroche, C. Serre, F. Millange, T. Loiseau and A. Percheron-Guégan, *Chem. Commun*., 2003, 2976.
177 M. Dincã and J. R. Long, *J. Am. Chem. Soc*., 2005, **127**, 9376.
178 O. K. Farha, A. M. Spokoyny, K. L. Mulfort, M. F. Hawthorne, C. A. Mirkin and J. T. Hupp, *J. Am. Chem. Soc*., 2007, **129**, 12680.
179 S. S. Kaye and J. R. Long, *J. Am. Chem. Soc*., 2005, **127**, 6506.
180 L. Reguera, C. P. Krap, J. Balmaseda and E. Reguera, *J. Phys. Chem. C*, 2008, **112**, 15893.
181 A. J. Robell, E. V. Ballou and M. Boudart, *J. Phys. Chem*., 1964, **68**, 2748.
182 Y. Li and R. T. Yang, *J. Am. Chem. Soc*., 2006, **128**, 726.
183 Y. Li and R. T. Yang, *J. Am. Chem. Soc*., 2006, **128**, 8136.
184 Y. Li and R. T. Yang, *Langmuir*, 2007, **23**, 12937.
185 Y. Li, F. H. Yang and R. T. Yang, *J. Phys. Chem. C*, 2007, **111**, 3405.
186 A. C. T. van Duin, S. Dasgupta, F. Lorant and W. A. Goddard III, *J. Phys. Chem. A*, 2001, **105**, 9396; A. C. T. van Duin, A. Strachan, S. Stewman, Q. S. Zhang, X. Xu and W. A. Goddard III, *J. Phys. Chem. A*, 2003, **107**, 3803; A. Strachan, A. C. T. van Duin, D. Chakraborty, S. Dasgupta and W. A. Goddard III, *Phys. Rev. Lett*., 2003, **91**, 098301; Q. Zhang, T. Çağın, A. van Duin and W. A. Goddard III, *Phys. Rev. B*, 2004, **69**, 045423; K. D. Nielson, A. C. T. van Duin, J. Oxgaard, W.-Q. Deng and W. A. Goddard III, *J. Phys. Chem. A*, 2005, **109**, 493; S. Cheung, W.-Q. Deng, A. C. T. van Duin and W. A. Goddard III, *J. Phys. Chem. A*, 2005, **109**, 851; S. S. Han, A. C. T. van Duin, W. A. Goddard III and H. M. Lee, *J. Phys. Chem. A*, 2005, **109**, 4575; S. S. Han, J. K. Kang, H. M. Lee, A. C. T. van Duin and W. A. Goddard III, *J. Chem. Phys*., 2005, **123**, 114703; W. Goddard III, B. Merinov, A. van Duin, T. Jacob, M. Blanco, V. Molinero, S. S. Jang and Y. H. Jang, *Mol. Simul*., 2006, **32**, 251; W. A. Goddard III, A. van Duin, K. Chenoweth, M.-J. Cheng, S. Pudar, J. Oxgaard, B. Merinov, Y. H. Jang and P. Persson, *Top. Catal*., 2006, **38**, 93; J. Ludwig, D. G. Vlachos, A. C. T. van Duin and W. A. Goddard III, *J. Phys. Chem. A*, 2006, **110**, 4274.

